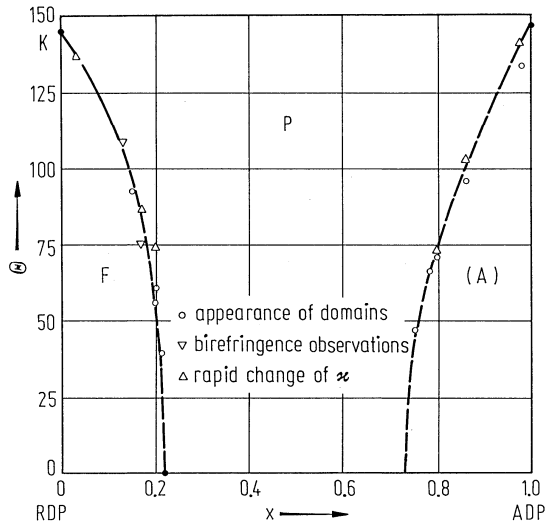

Fig. 33B-5-001. $Rb_{1-x}(NH_4)_xH_2PO_4$ (RADP). Θ vs. x [85Cou].

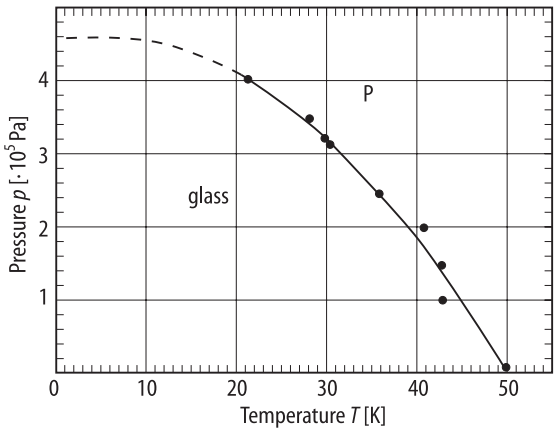

Fig. 33B-5-002. $Rb_{1-x}(NH_4)_xH_2PO_4$ (RADP, x = 0.25). Phase diagram in p–T plane determined with neutron diffuse scattering [92Mou].

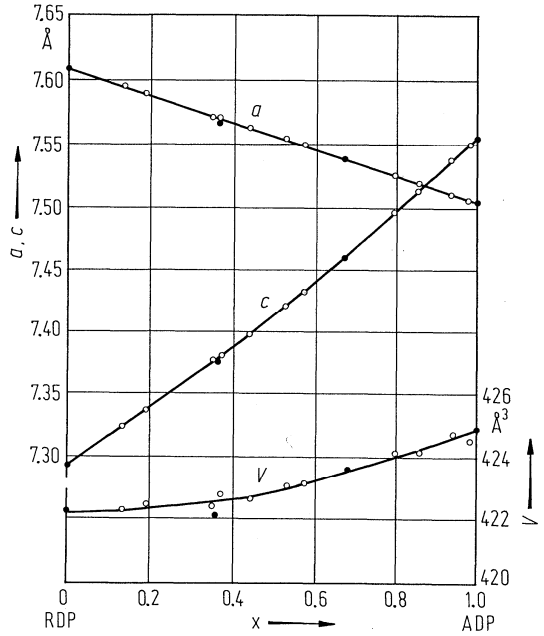

Fig. 33B-5-003. $Rb_{1-x}(NH_4)_xH_2PO_4$ (RADP). *a*, *c*, *V* vs. x at RT [85Cou]. *V*: volume of the unit cell.

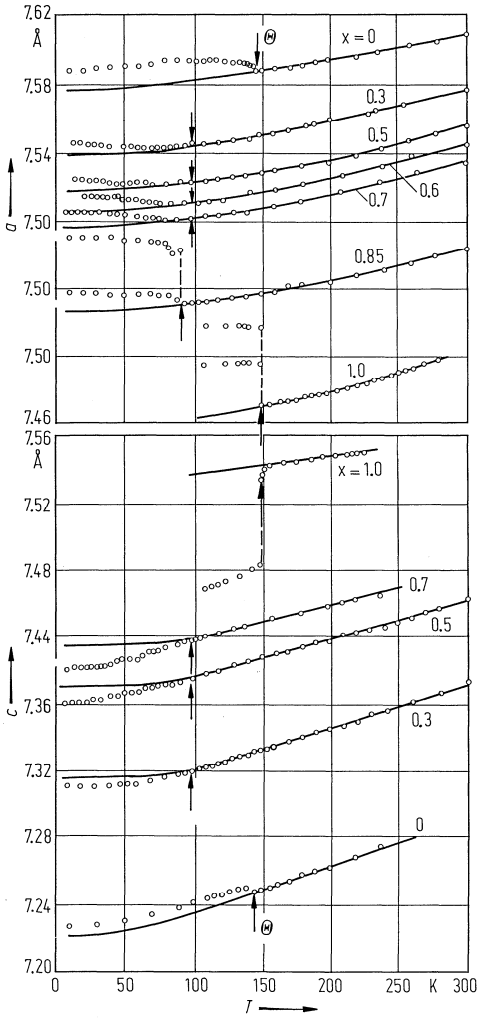

Fig. 33B-5-004. $Rb_{1-x}(NH_4)_xH_2PO_4$ (RADP). *a*, *c* vs. *T* [86Hay]. Parameter: x.

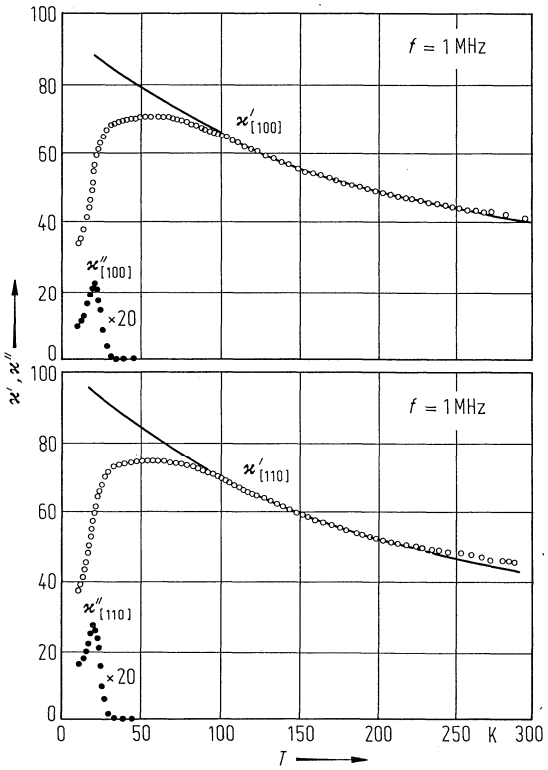

Fig. 33B-5-005. $Rb_{1-x}(NH_4)_xH_2PO_4$ (RADP, x = 0.39). $\kappa'_{[100]}$, $\kappa''_{[100]}$, $\kappa'_{[110]}$, $\kappa''_{[110]}$ vs. T [86Lee].

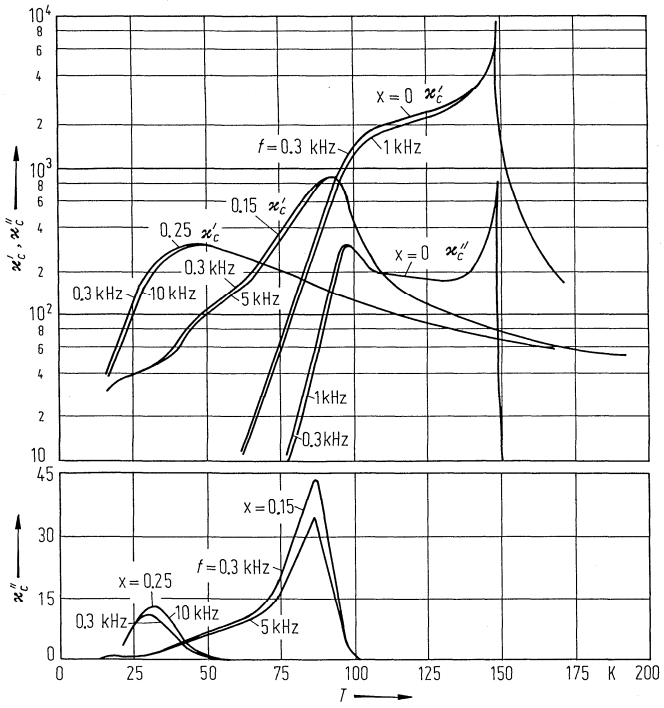

Fig. 33B-5-006. $Rb_{1-x}(NH_4)_xH_2PO_4$ (RADP). κ'_c, κ''_c vs. T [85Tak]. Parameters: x, f.

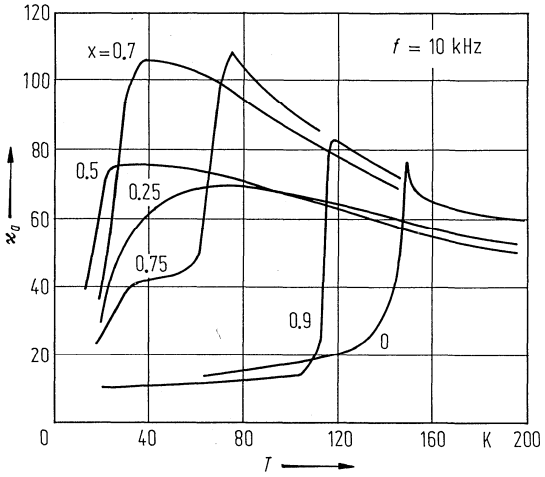

Fig. 33B-5-007. $Rb_{1-x}(NH_4)_xH_2PO_4$ (RADP). $\varkappa_a$ vs. T [85Tak]. Parameter: x.

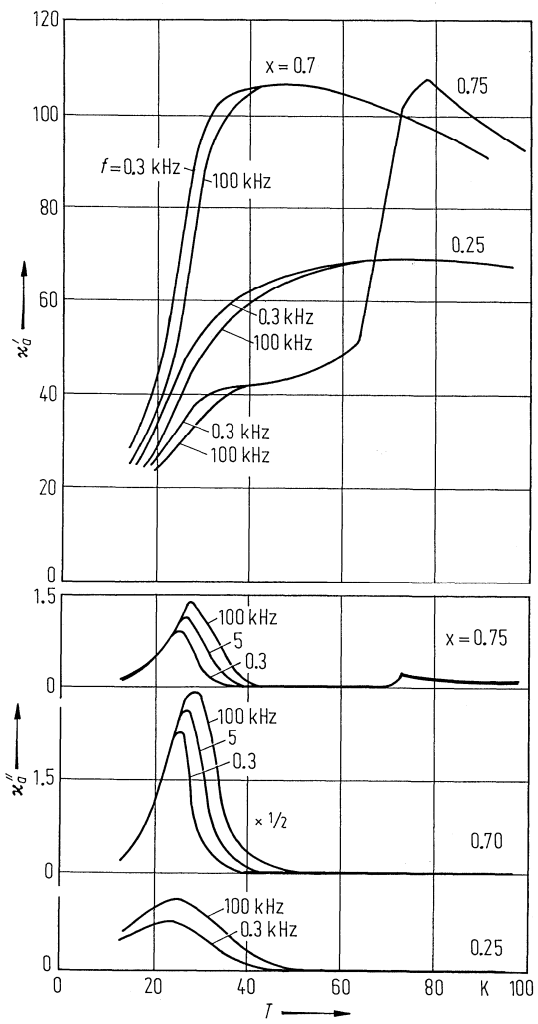

Fig. 33B-5-008. $Rb_{1-x}(NH_4)_xH_2PO_4$ (RADP). κ_a', κ_a'' vs. T [85Tak]. Parameters: f, x.

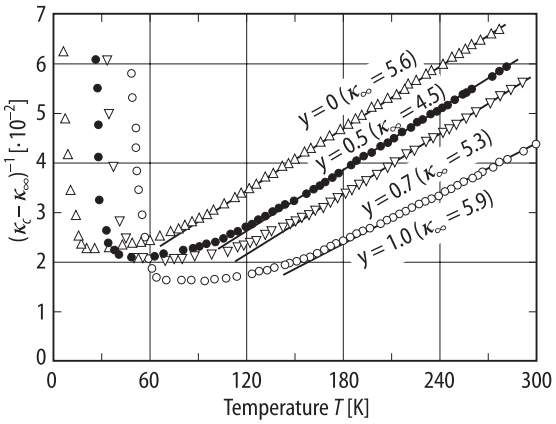

Fig. 33B-5-009. $Rb_{1-x}[N(H_{1-y}D_y)_4]_x(H_{1-y}D_y)_2PO_4$ (RADP–DRADP, x = 0.5). $(\kappa_c - \kappa_\infty)^{-1}$ vs. T [91HeP1]. Parameter: y. f = 10 kHz. κ_∞: high frequency limit of κ_c.

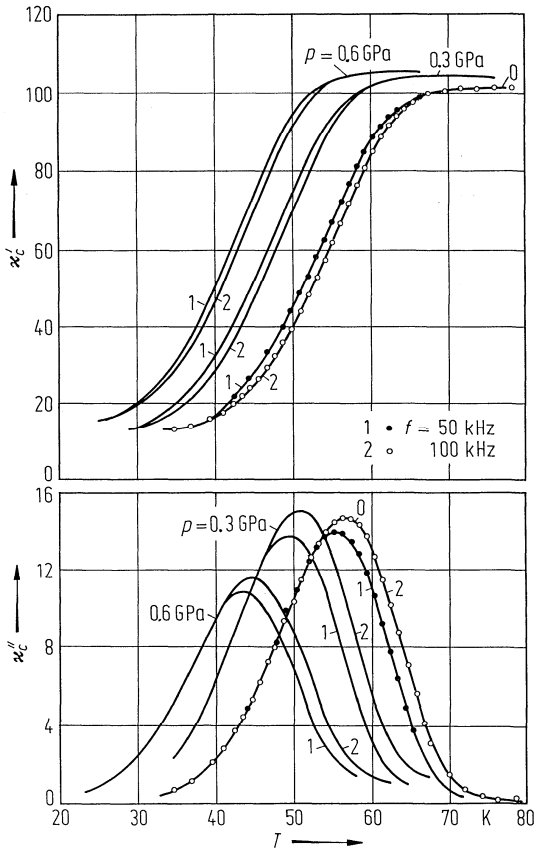

Fig. 33B-5-010. $Rb_{1-x}[N(H_{1-y}D_y)_4]_x(H_{1-y}D_y)_2PO_4$ (x = 0.48, y = 0.72). κ_c', κ_c'' vs. T at 50 kHz and 100 kHz [86Sam]. Parameter: p.

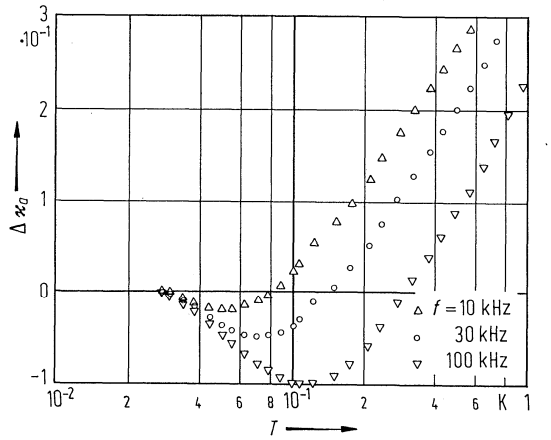

Fig. 33B-5-011. $Rb_{1-x}(NH_4)_xH_2PO_4$ (RADP, x = 0.75). $\Delta\kappa_a$ vs. T [85Miu]. Parameter: f. $\Delta\kappa_a$: change in the dielectric constant along the a axis.

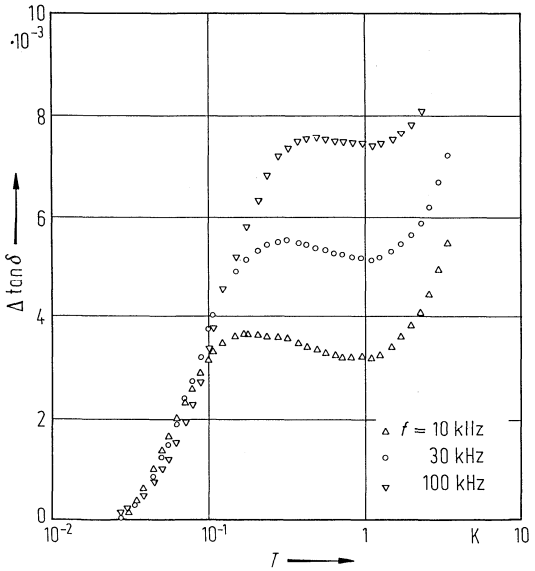

Fig. 33B-5-012. $Rb_{1-x}(NH_4)_xH_2PO_4$ (RADP, x = 0.75). $\Delta \tan \delta$ vs. T [85Miu]. Parameter: f. $\Delta \tan \delta$: change in the dielectric loss tangent along the a axis.

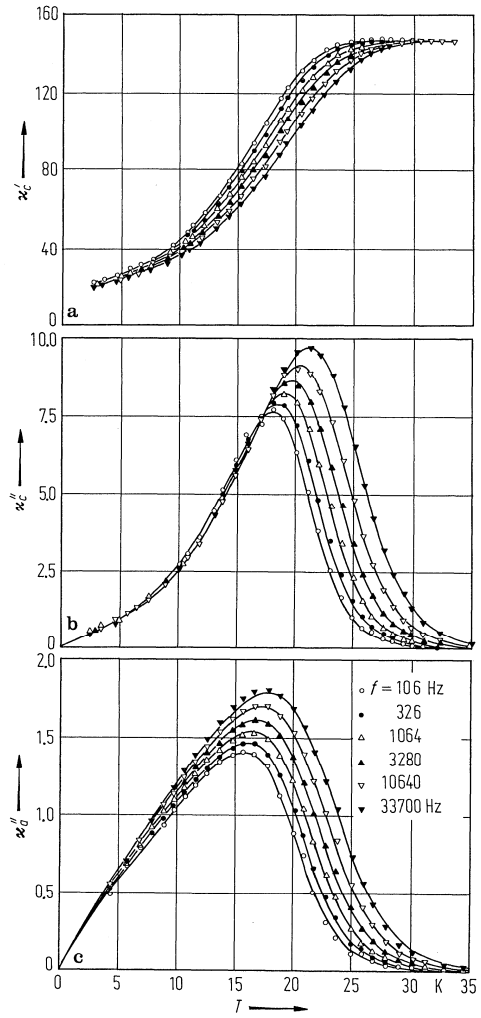

Fig. 33B-5-013. $Rb_{1-x}(NH_4)_xH_2PO_4$ (RADP, x = 0.35). κ_c', κ_c'', κ_a'' vs. T [84Cou]. Parameter: f. (**a**) κ_c'. (**b**) κ_c''. (**c**) κ_a''.

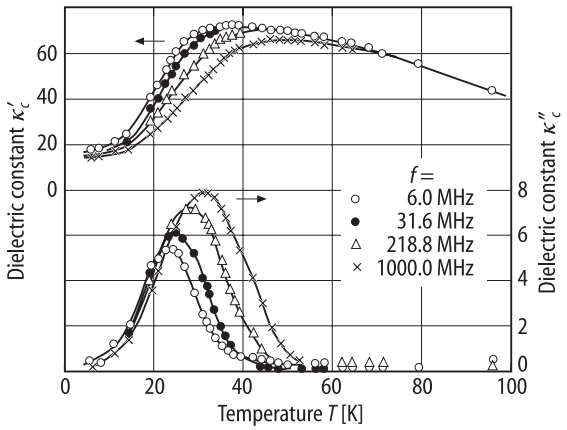

Fig. 33B-5-014. $Rb_{1-x}(NH_4)_xH_2PO_4$ (RADP, x = 0.35). κ_c', κ_c'' vs. T [90HeP]. Parameter: f.

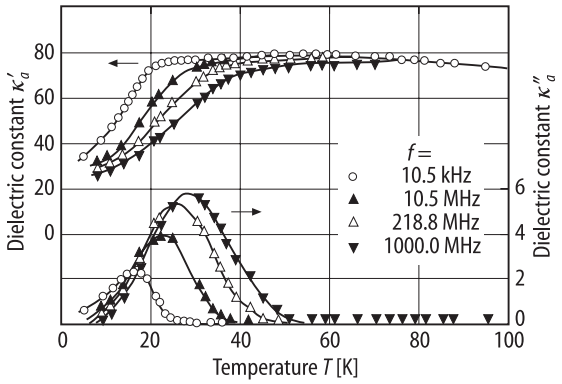

Fig. 33B-5-015. $Rb_{1-x}(NH_4)_xH_2PO_4$ (RADP, x = 0.35). κ_a', κ_a'' vs. T [90HeP]. Parameter: f.

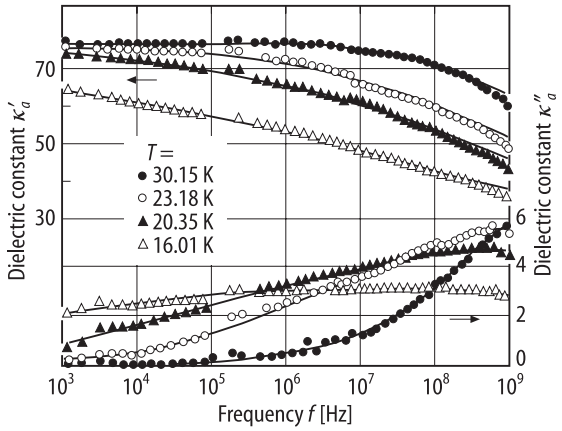

Fig. 33B-5-016. $Rb_{1-x}(NH_4)_xH_2PO_4$ (RADP, x = 0.35). κ_a', κ_a'' vs. f [90HeP]. Parameter: T.

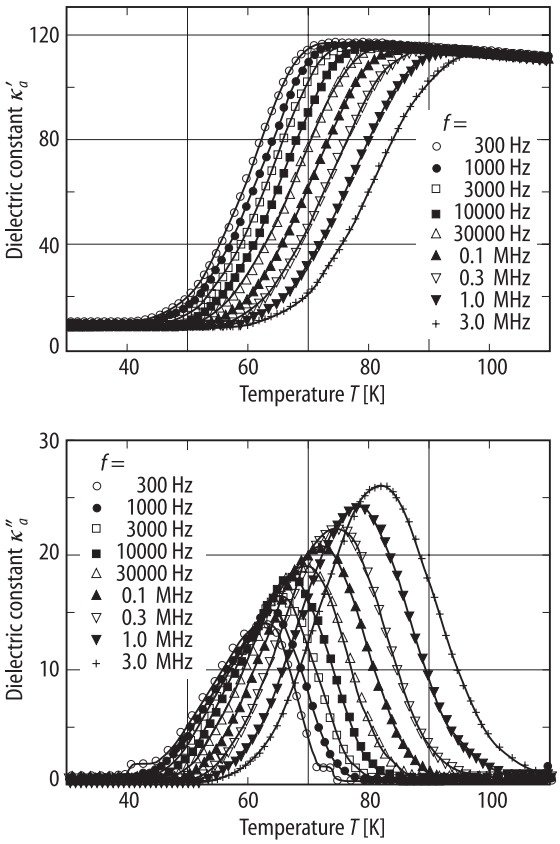

Fig. 33B-5-017. $Rb_{1-x}(ND_4)_xD_2PO_4$. κ'_a, κ''_a vs. T [86Cou2]. Parameter: f.

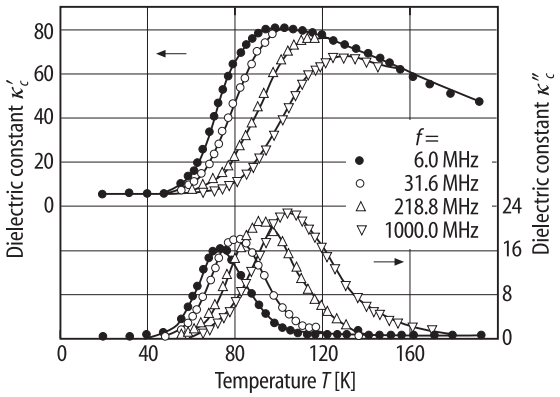

Fig. 33B-5-018. $Rb_{1-x}(ND_4)_xD_2PO_4$ (DRADP, x = 0.35). κ'_c, κ''_c vs. T [90HeP]. Parameter: f.

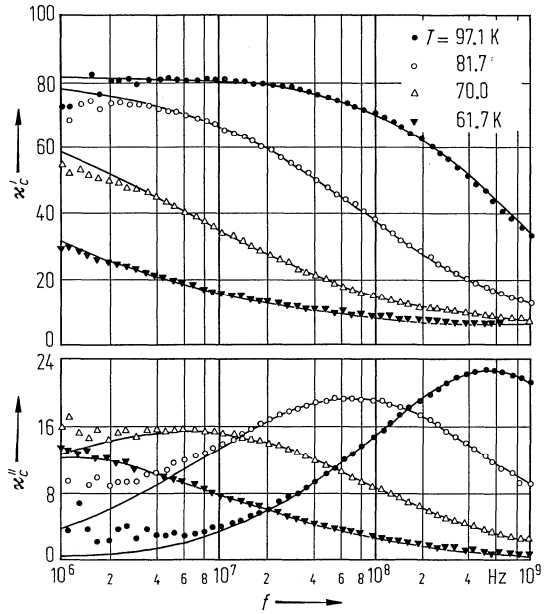

Fig. 33B-5-019. $Rb_{1-x}(ND_4)_xD_2PO_4$ (DRADP, x = 0.35). κ_c', κ_c'' vs. f [88HeP]. Parameter: T.

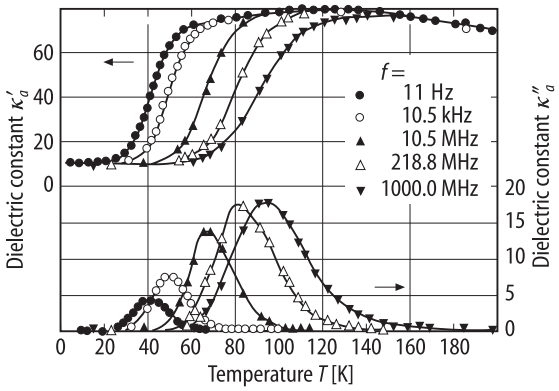

Fig. 33B-5-020. $Rb_{1-x}(ND_4)_xD_2PO_4$ (DRADP, x = 0.35). κ_a', κ_a'' vs. T [90HeP]. Parameter: f.

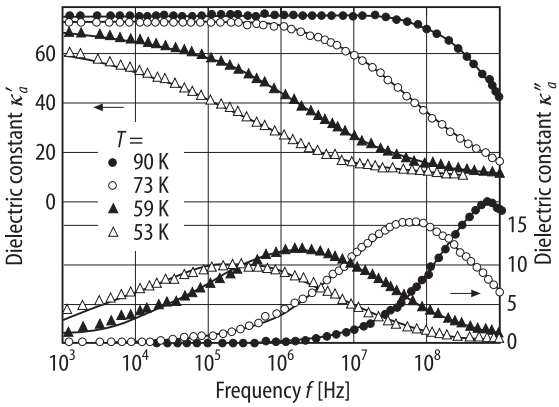

Fig. 33B-5-021. $Rb_{1-x}(ND_4)_xD_2PO_4$ (DRADP, x = 0.35). κ_a', κ_a'' vs. f [90HeP]. Parameter: T.

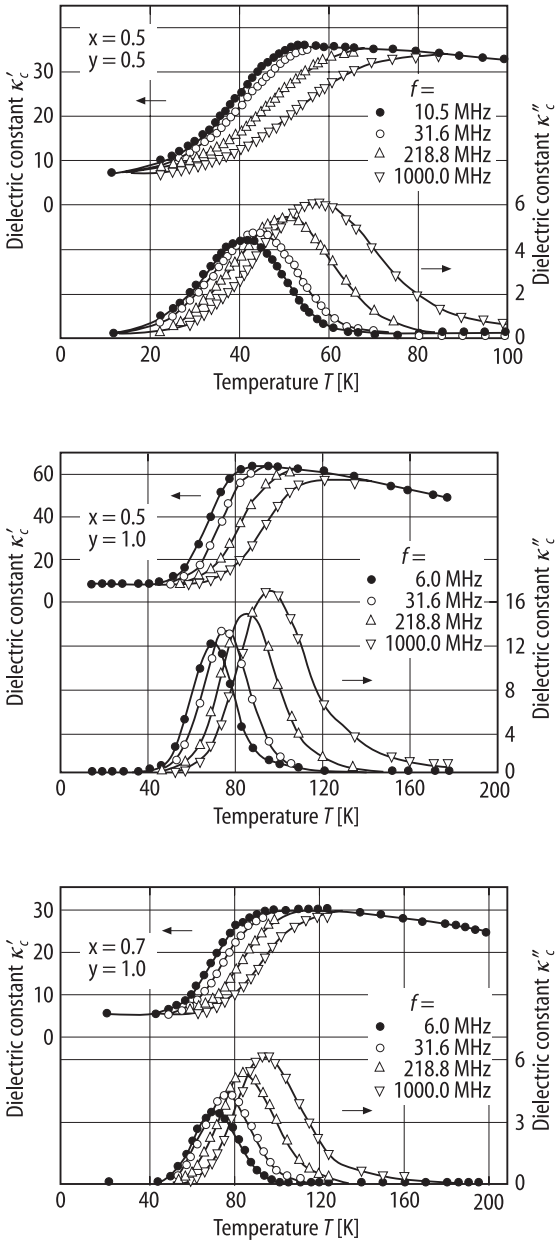

Fig. 33B-5-022. $Rb_{1-x}[N(H_{1-y}D_y)_4]_x(H_{1-y}D_y)_2PO_4$. κ_c', κ_c'' vs. T [91HeP2]. Parameter: x, y, f.

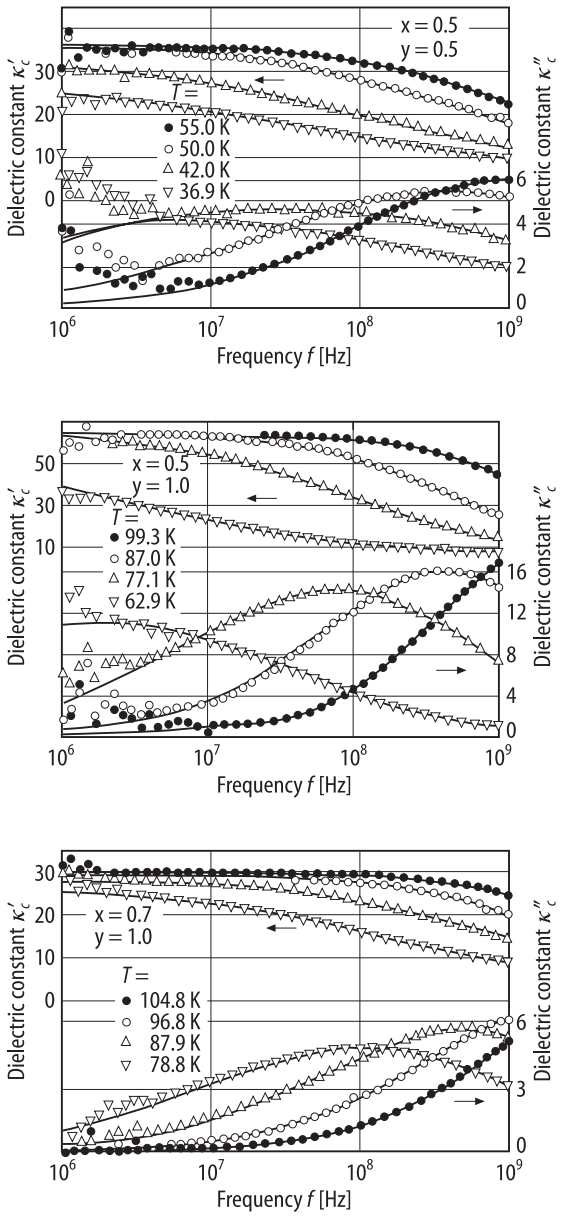

Fig. 33B-5-023. $Rb_{1-x}[N(H_{1-y}D_y)_4]_x(H_{1-y}D_y)_2PO_4$. κ_c', κ_c'' vs. f [91HeP2]. Parameter: x, y, T.

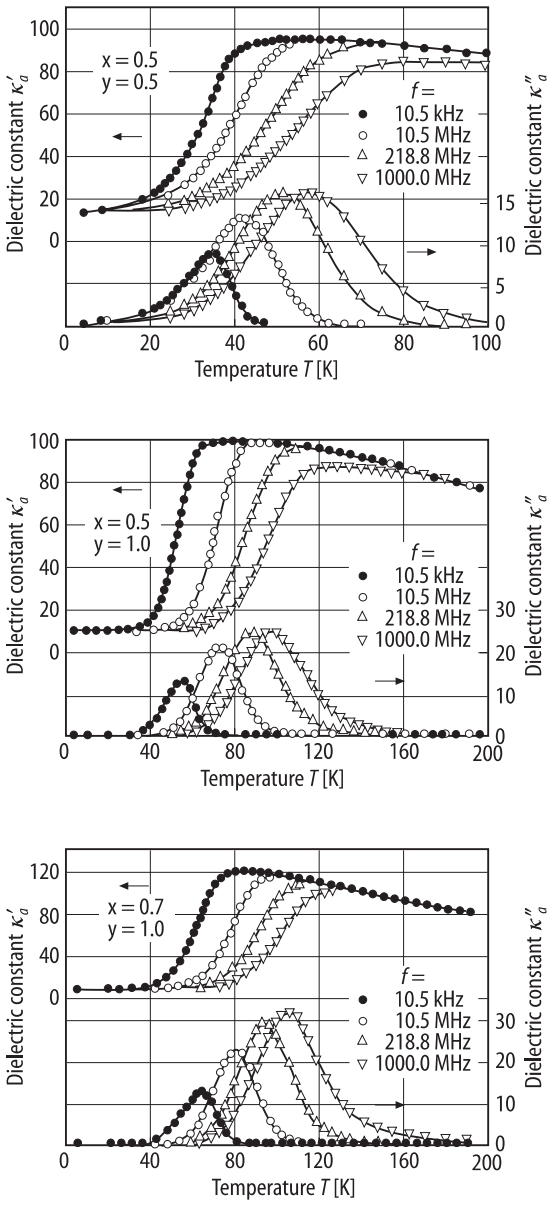

Fig. 33B-5-024. $Rb_{1-x}[N(H_{1-y}D_y)_4]_x(H_{1-y}D_y)_2PO_4$. κ'_a, κ''_a vs. T [91HeP2]. Parameter: x, y, f.

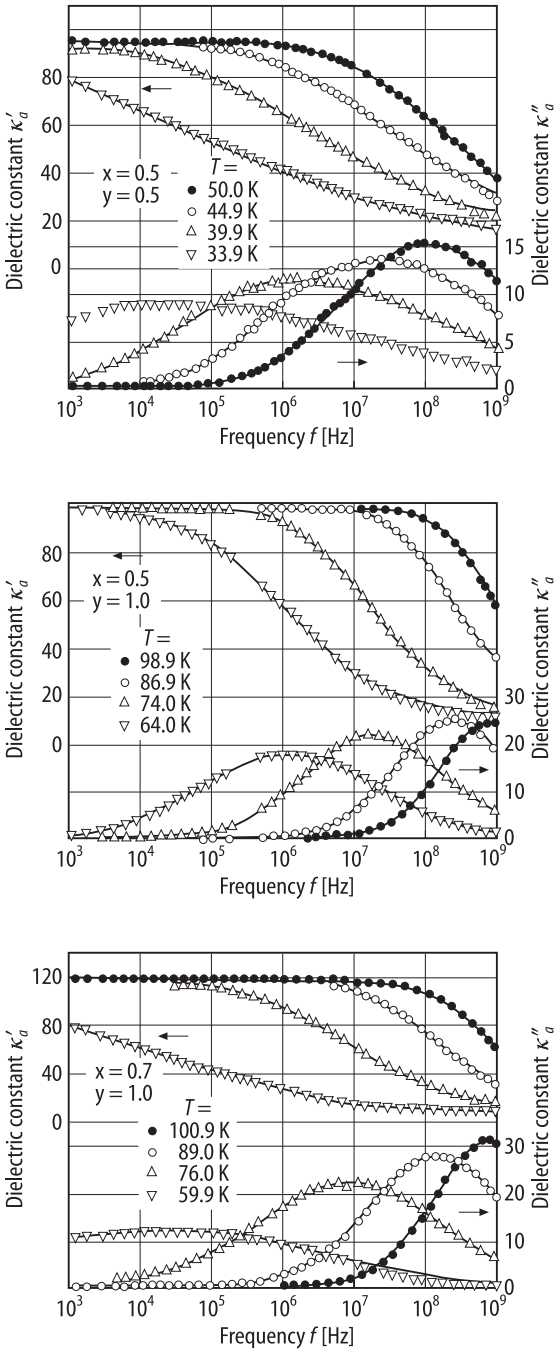

Fig. 33B-5-025. $Rb_{1-x}[N(H_{1-y}D_y)_4]_x(H_{1-y}D_y)_2PO_4$. κ'_a, κ''_a vs. f [91HeP2]. Parameter: x, y, T.

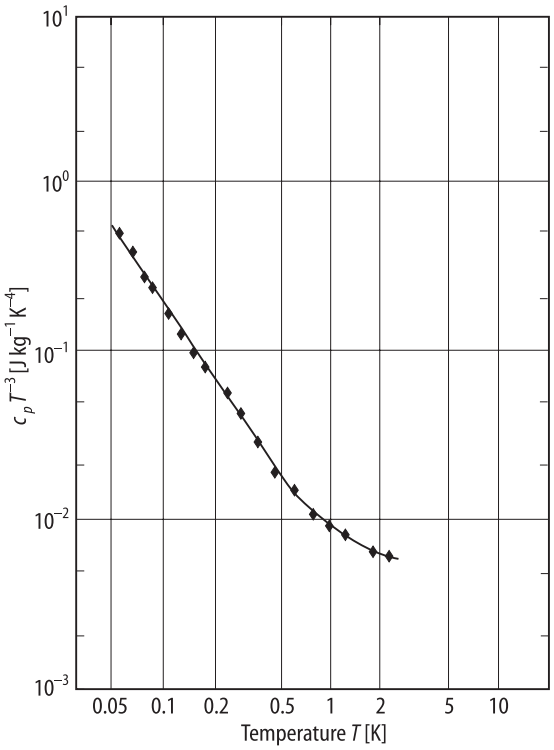

Fig. 33B-5-026. $Rb_{1-x}(NH_4)_xH_2PO_4$ (RADP, x = 0.35). c_p/T^3 vs. T [92Ber]. c_p: specific heat capacity at constant pressure.

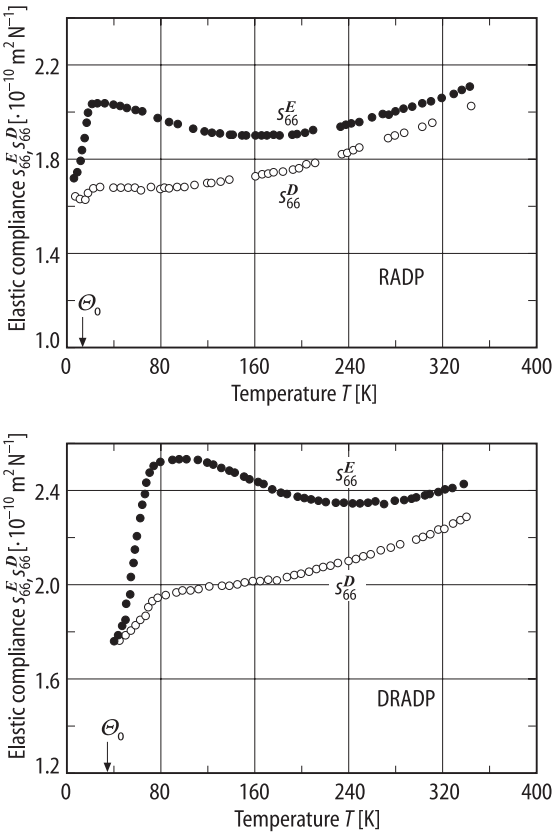

Fig. 33B-5-027. $Rb_{1-x}(NH_4)_xH_2PO_4$ (RADP, x = 0.5), $Rb_{1-x}(ND_4)_xD_2PO_4$ (DRADP, x = 0.5). s_{66}^E, s_{66}^D vs. T [91HeP1]. Θ_0: Vogel-Fulcher temperature determined by dielectric measurements.

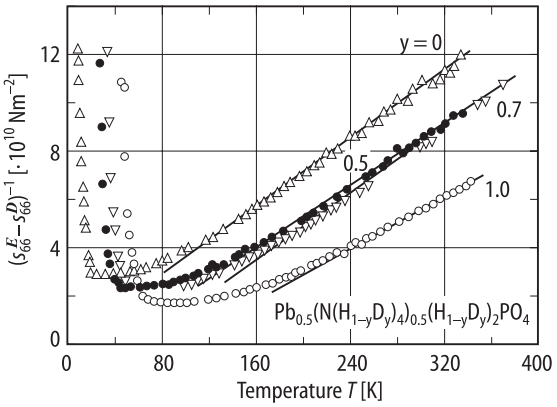

Fig. 33B-5-028. $Rb_{1-x}[N(H_{1-y}D_y)_4]_x(H_{1-y}D_y)_2PO_4$. (RADP–DRADP, x = 0.5). $\left(s_{66}^E - s_{66}^D\right)^{-1}$ vs. T [91HeP1]. Parameter: deuteration rate y.

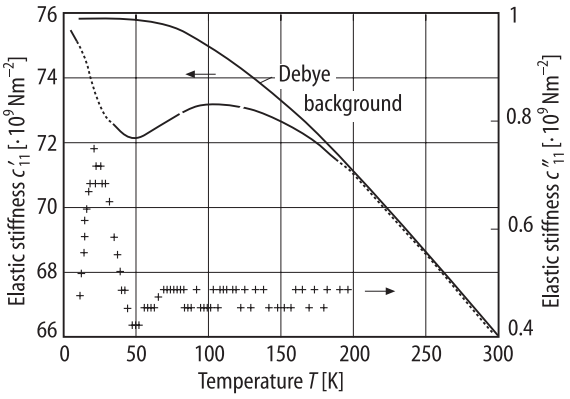

Fig. 33B-5-029. $Rb_{1-x}(NH_4)_xH_2PO_4$ (RADP, x = 0.35). c'_{11}, c''_{11} vs. T [88San]. c'_{11}, c''_{11} : real and imaginary parts of elastic stiffness c_{11}. f = 25 MHz. Solid line: Debye background fitted for T > 200 K with the Debye temperature Θ_D = 400 K.

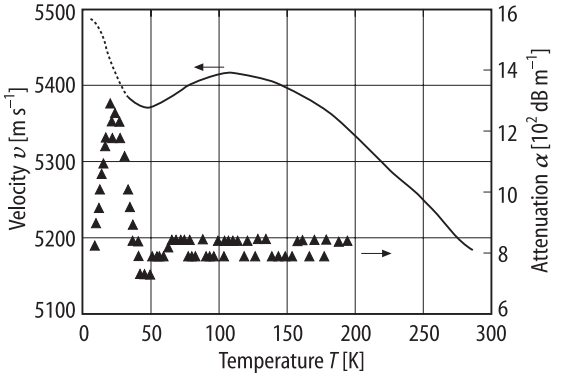

Fig. 33B-5-030. $Rb_{1-x}(NH_4)_xH_2PO_4$ (RADP, x = 0.55). v, α vs. T [88San]. v: velocity of longitudinal acoustic wave propagating along [100]. α: attenuation coefficient. f = 25MHz. Full triangle: velocity obtained from Brillouin scattering.

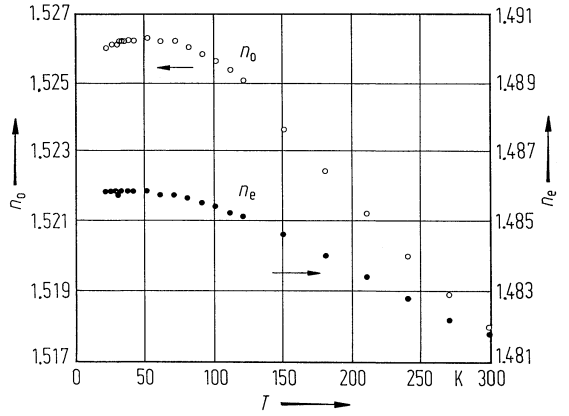

Fig. 33B-5-031. $Rb_{1-x}(NH_4)_xH_2PO_4$ (RADP, x = 0.35). n_o, n_e vs. T [86Cou1]. λ = 514.5 nm.

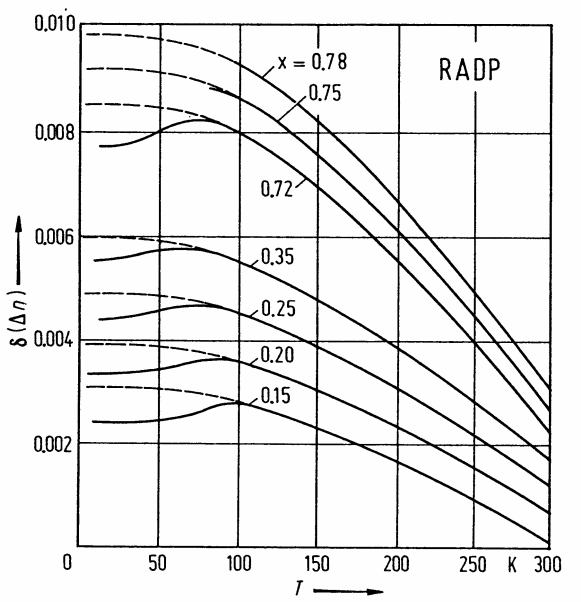

Fig. 33B-5-032. $Rb_{1-x}(NH_4)_xH_2PO_4$ (RADP). $\delta(\Delta n)$ vs. T [87Cou]. Parameter: x. λ = 632.8 nm. $\delta(\Delta n)$: change in birefringence $\Delta n = n_o - n_e$.

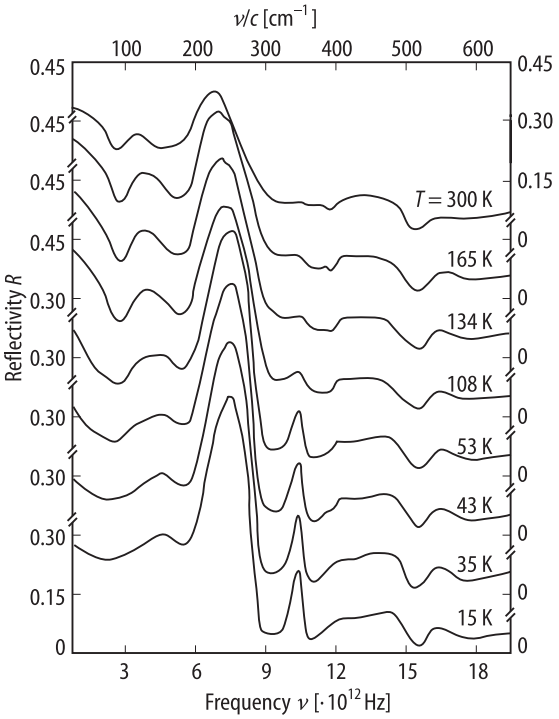

Fig. 33B-5-033. $Rb_{1-x}(NH_4)_xH_2PO_4$ (RADP, x = 0.5). R vs. ν [91Pet]. Parameter: T. $\boldsymbol{E} \parallel \boldsymbol{c}$.

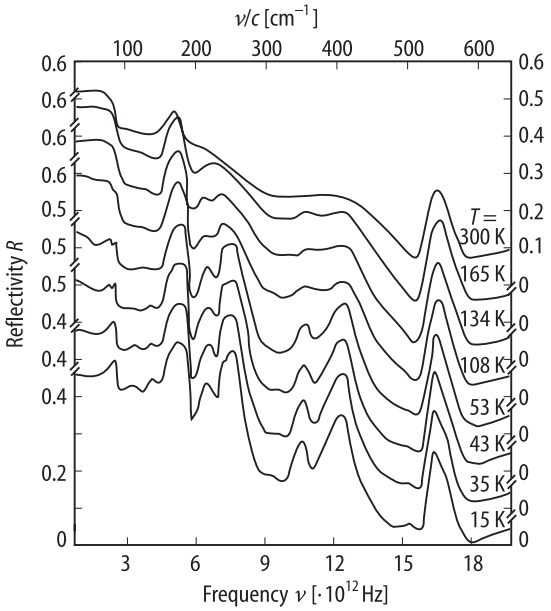

Fig. 33B-5-034. $Rb_{1-x}(NH_4)_xH_2PO_4$ (RADP, x = 0.5). R vs. ν [91Pet]. Parameter: T. $\boldsymbol{E} \perp \boldsymbol{c}$.

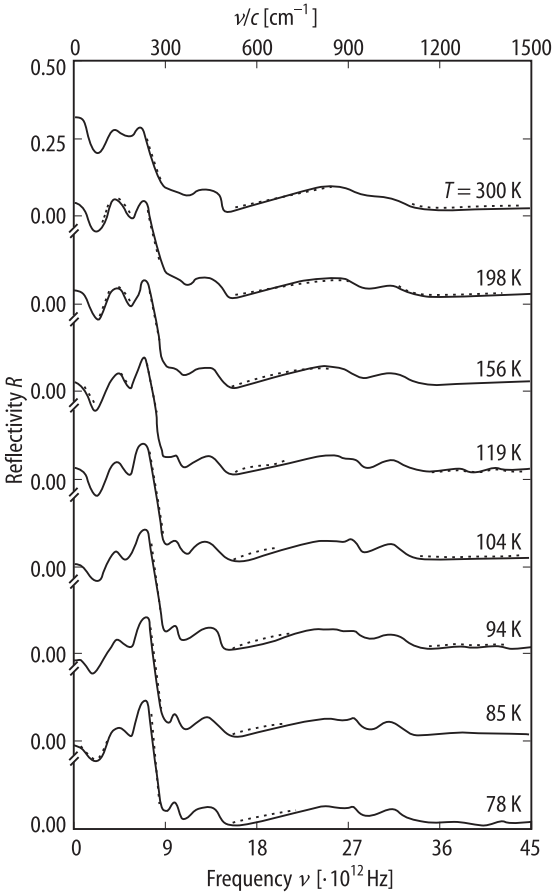

Fig. 33B-5-035. $Rb_{1-x}(NH_4)_xH_2PO_4$ (RADP, x = 0.35). R vs. ν [92Sim]. Parameter: T. $\boldsymbol{E} \parallel \boldsymbol{c}$. Dots: experimental; full lines: best simulation with the factorized form of the dielectric function.

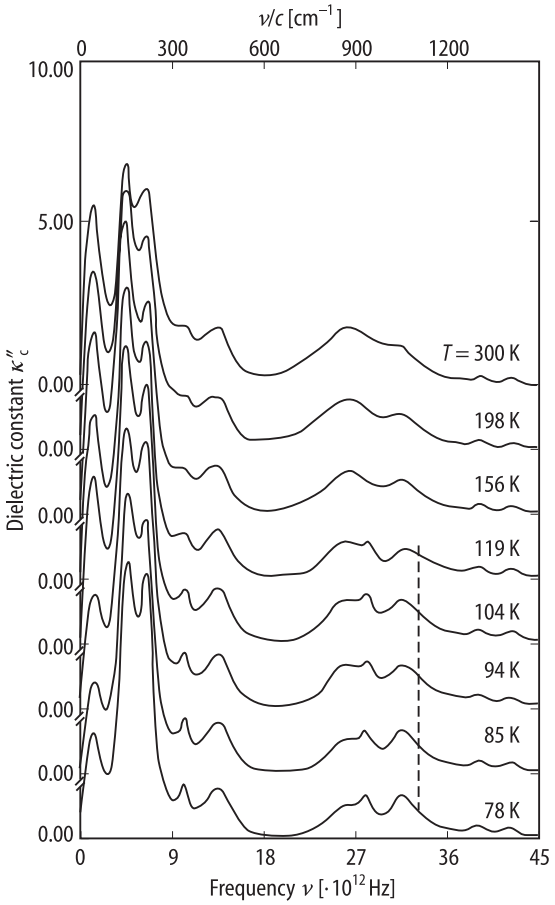

Fig. 33B-5-036. $Rb_{1-x}(NH_4)_xH_2PO_4$ (RADP, x = 0.35). κ_c'' vs. ν determined from far-infrared reflectivity [92Sim]. Parameter: *T*.

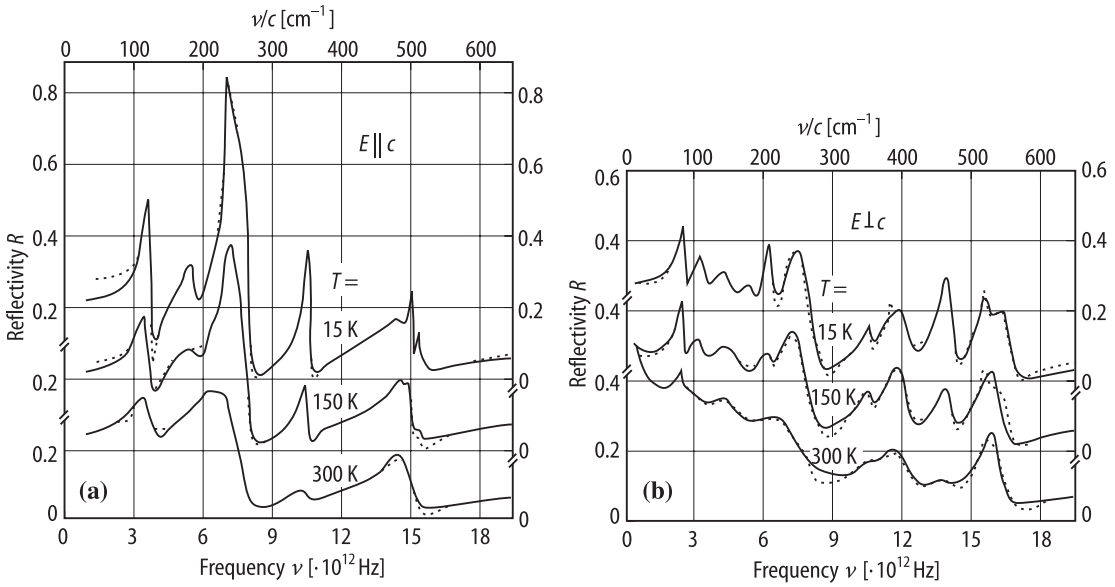

Fig. 33B-5-037. $Rb_{1-x}(ND_4)_xD_2PO_4$ (DRADP, x = 0.25). *R* vs. ν [94Kam]. Parameter: *T*. Dashed line: experiment; full lines: best fit to the factorized form of the dielectric function. (**a**) $\boldsymbol{E} \parallel \boldsymbol{c}$, (**b**) $\boldsymbol{E} \perp \boldsymbol{c}$.

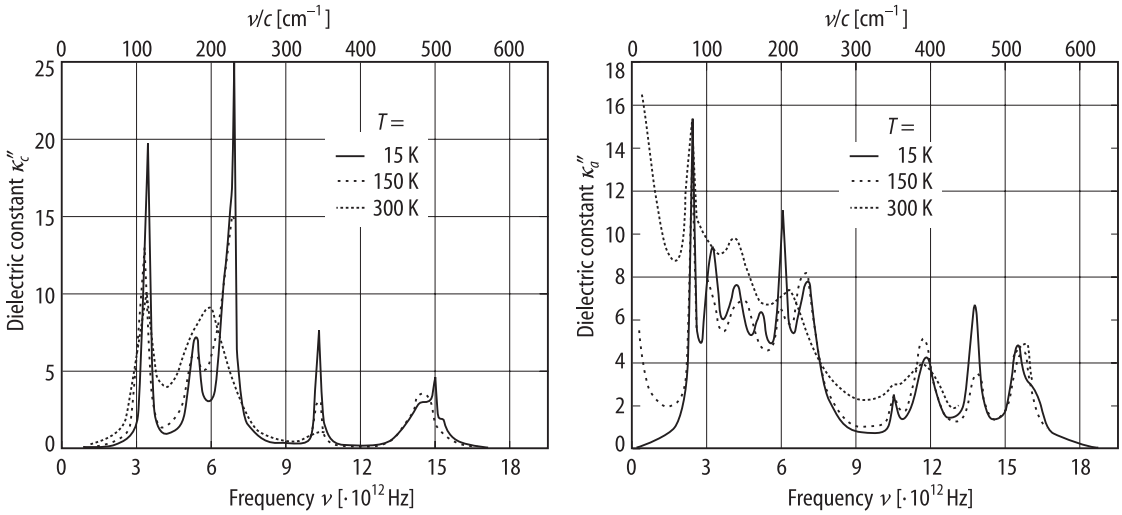

Fig. 33B-5-038. $Rb_{1-x}(ND_4)_xD_2PO_4$ (DRADP, x = 0.25). κ''_c, κ''_a vs. ν determined from far-infrared reflectivity [94Kam]. Parameter: *T*.

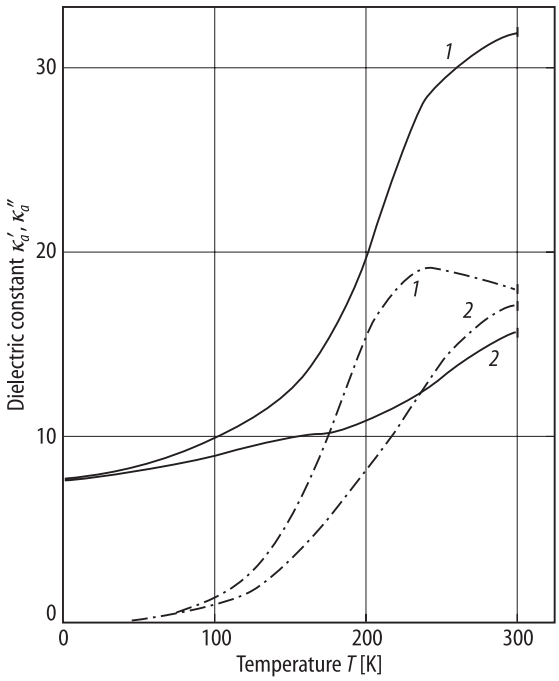

Fig. 33B-5-039. $Rb_{1-x}(ND_4)_xD_2PO_4$ (DRADP, x = 0.25). κ'_a, κ''_a vs. *T* in far-infrared region [94Kam]. Full line: κ'_a. Chain line: κ''_a. *1*: $\nu = 21 \cdot 10^{10}$ Hz, *2*: $\nu = 60 \cdot 10^{10}$ Hz.

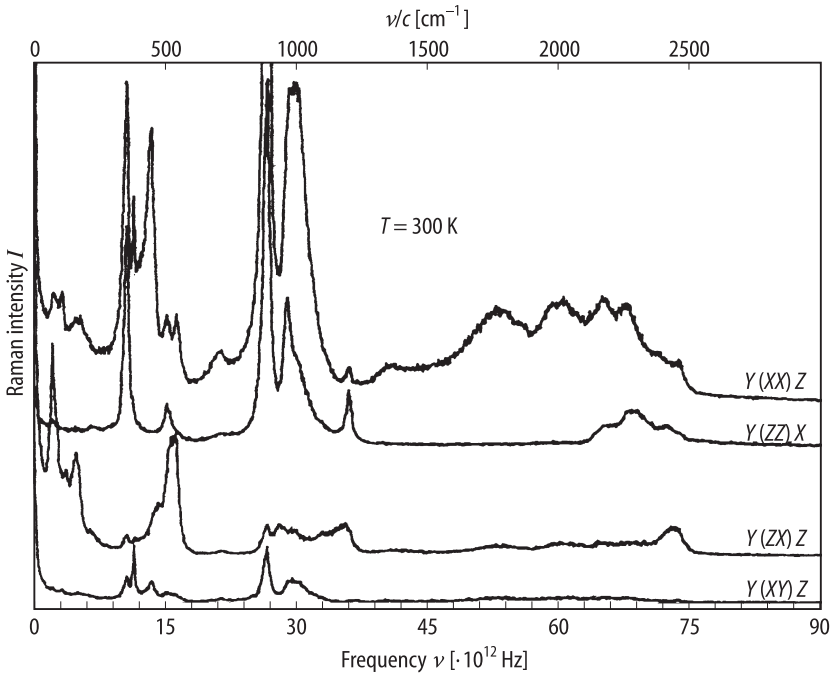

Fig. 33B-5-040. $Rb_{1-x}(ND_4)_xD_2PO_4$ (DRADP, x = 0.25). I vs. ν [96Yuz]. I: Raman scattering intensity. T = 300 K.

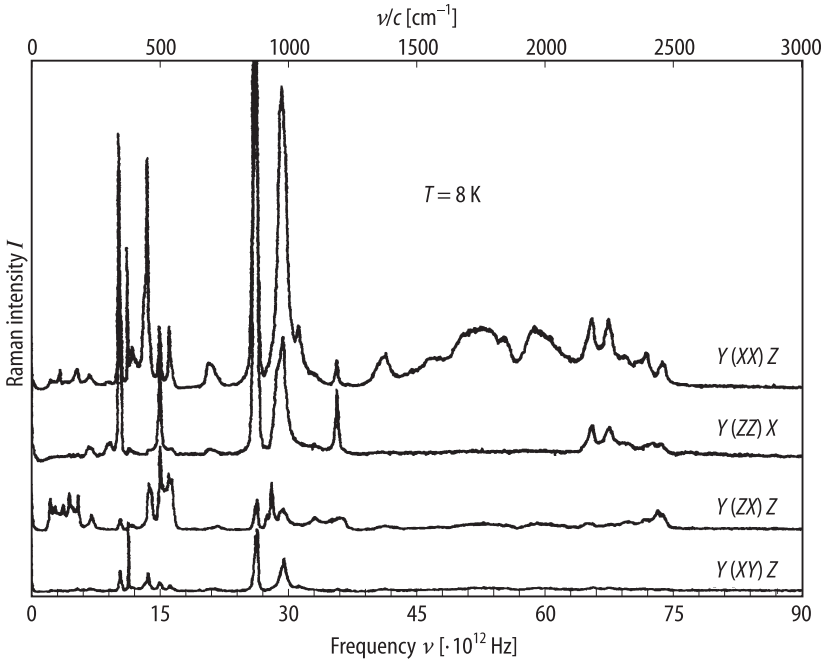

Fig. 33B-5-041. $Rb_{1-x}(ND_4)_xD_2PO_4$ (DRADP, x = 0.25). I vs. ν [96Yuz]. I: Raman scattering intensity. T = 8 K.

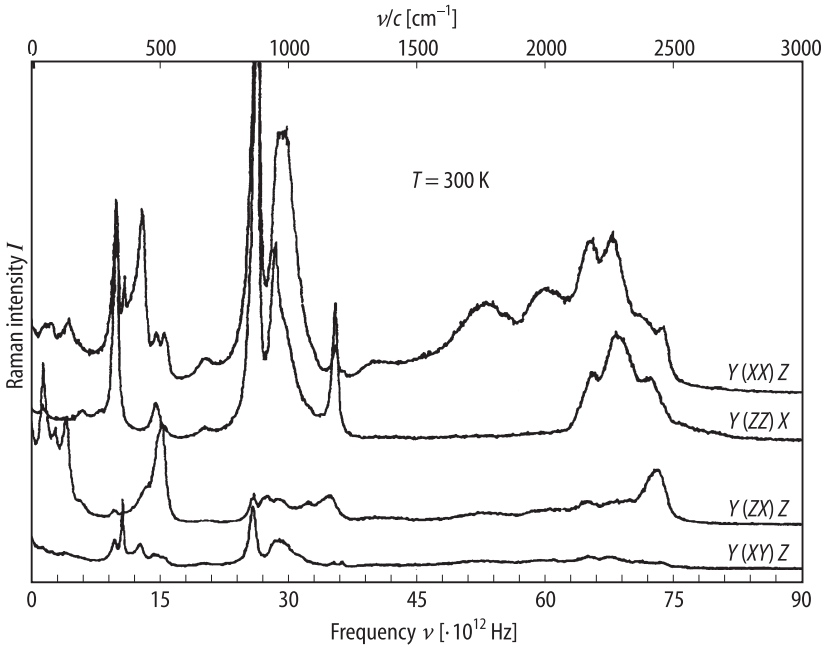

Fig. 33B-5-042. $Rb_{1-x}(ND_4)_xD_2PO_4$ (DRADP, x = 0.50). *I* vs. ν [95Yuz]. *I*: Raman scattering intensity. $T = 300$ K.

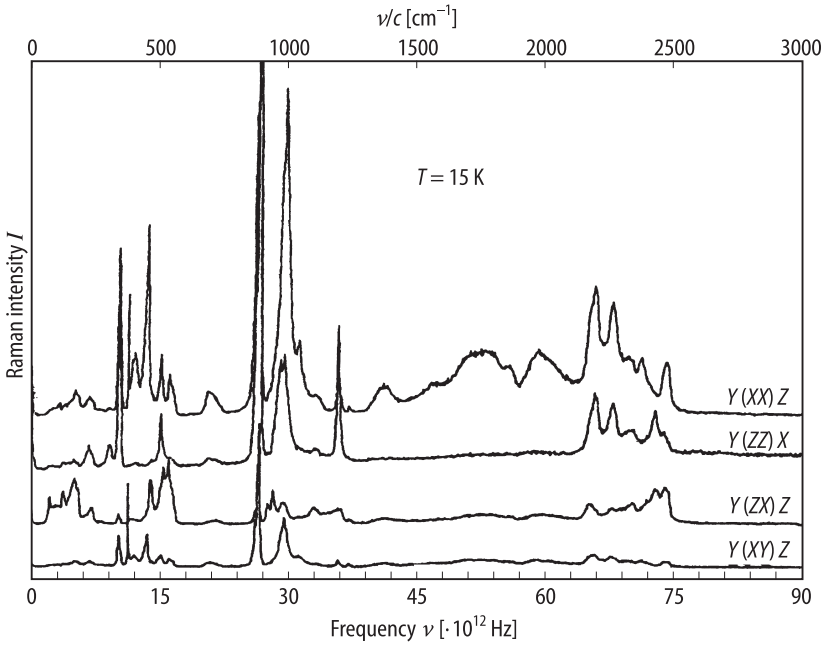

Fig. 33B-5-043. $Rb_{1-x}(ND_4)_xD_2PO_4$ (DRADP, x = 0.50). *I* vs. ν [95Yuz]. *I*: Raman scattering intensity. $T = 15$ K.

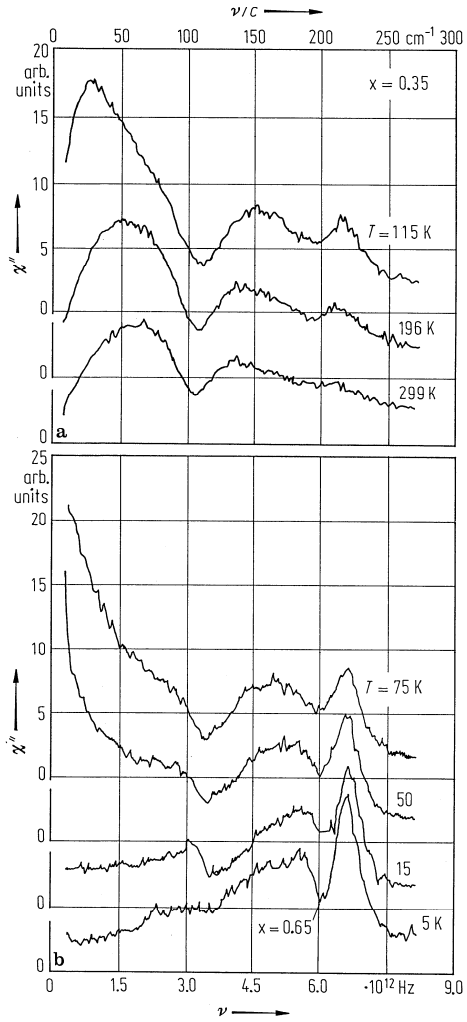

Fig. 33B-5-044. $Rb_{1-x}(NH_4)_xH_2PO_4$ (RADP, x = 0.35). χ'' vs. ν [86Cou3]. Parameter: *T*. χ'': Raman susceptibility in *X*(*YX*)*Y* scattering geometry. The curve of *T* = 5 K is for x = 0.65 (the x = 0.35 spectrum does not change from 15 K to 5 K).

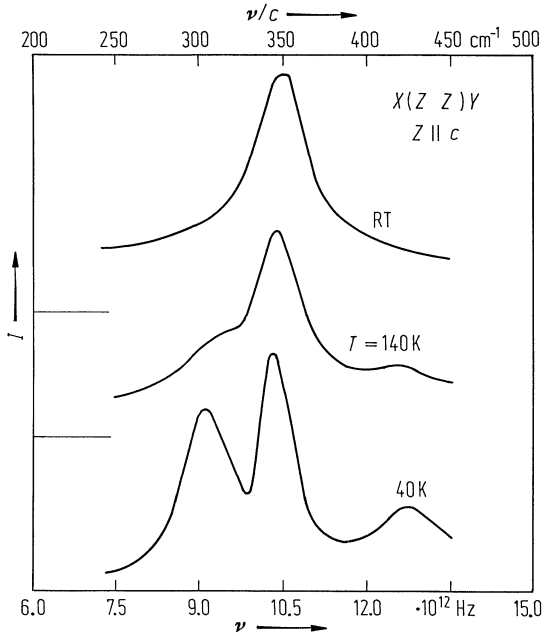

Fig. 33B-5-045. $Rb_{1-x}(NH_4)_xH_2PO_4$ (RADP, x = 0.7). *I* vs. ν [88Hat]. Parameter: *T*. *I*: Raman scattering intensity.

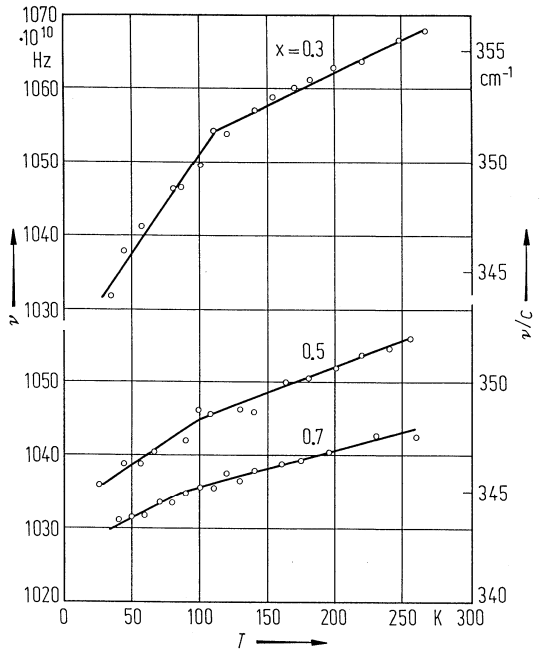

Fig. 33B-5-046. $Rb_{1-x}(NH_4)_xH_2PO_4$ (RADP). ν vs. *T* [88Hat]. Parameter: x. ν: Raman shift of E mode of PO_4 tetrahedron.

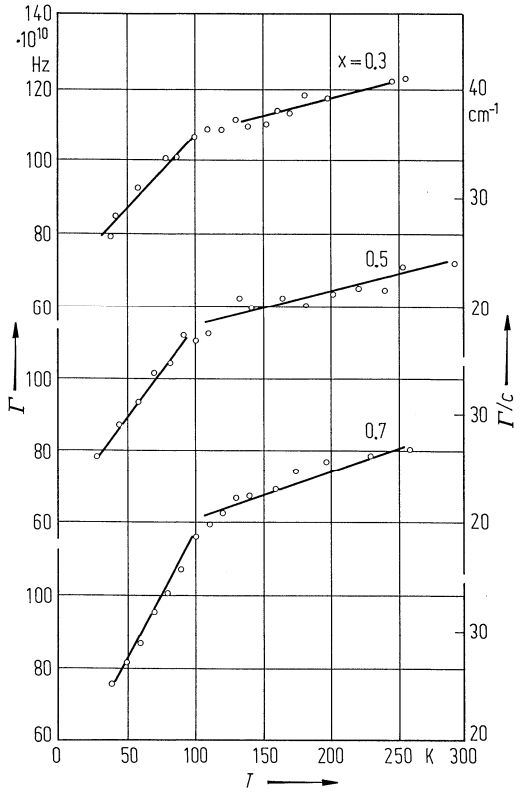

Fig. 33B-5-047. $Rb_{1-x}(NH_4)_xH_2PO_4$ (RADP). Γ vs. T [88Hat]. Parameter: x. Γ: full width at half maximum of E mode of PO_4 tetrahedron shown in Fig. 33B-5-045.

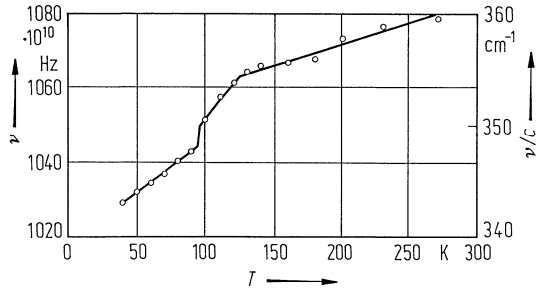

Fig. 33B-5-048. $Rb_{1-x}(NH_4)_xH_2PO_4$ (RADP, x = 0.2). ν vs. T [88Hat]. ν: Raman shift of E mode of PO_4 tetrahedron.

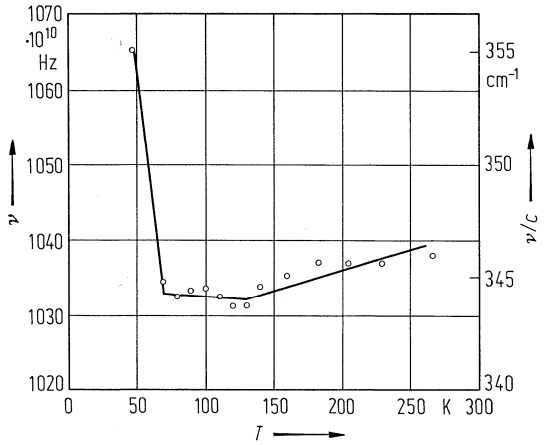

Fig. 33B-5-049. $Rb_{1-x}(NH_4)_xH_2PO_4$ (RADP, x = 0.8). ν vs. T [88Hat]. ν: Raman shift of E mode of PO_4 tetrahedron.

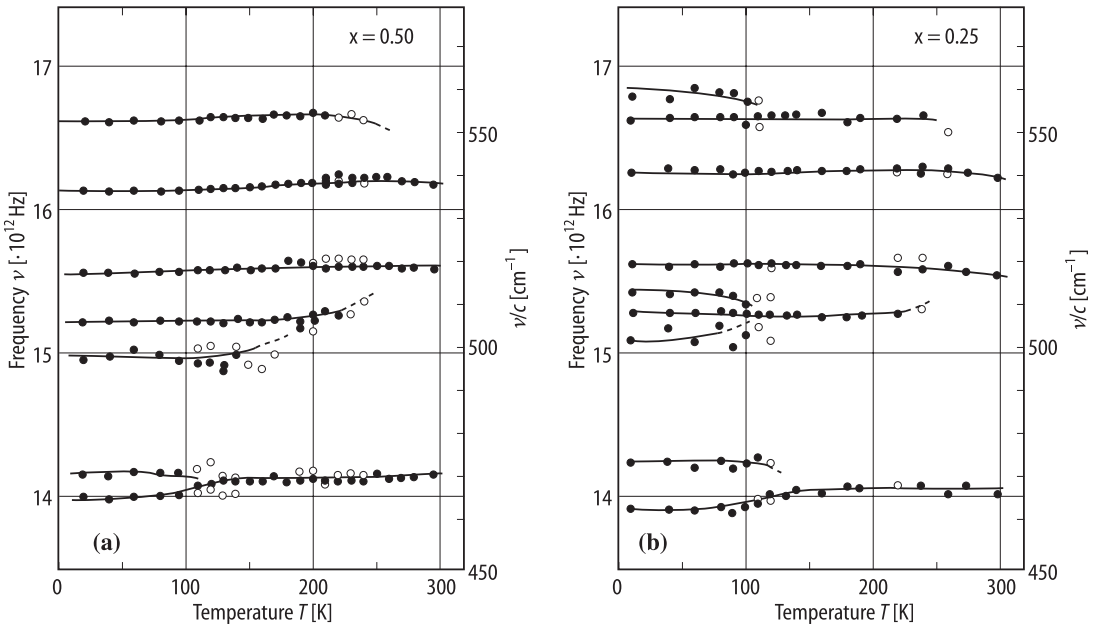

Fig. 33B-5-050. $Rb_{1-x}(ND_4)_xD_2PO_4$ (DRADP, x = 0.25, 0.50). ν vs. T [96Yuz]. ν: Raman frequency shift of $Y(ZX)Z$ geometry around $15 \cdot 10^{12}$ Hz (500 cm^{-1}) determined by multi-oscillator (Lorentzian) fits. Open circles: fits with a smaller number of Lorentzians. (**a**) x = 0.50, (**b**) x = 0.25. See Table 33B-5-002.

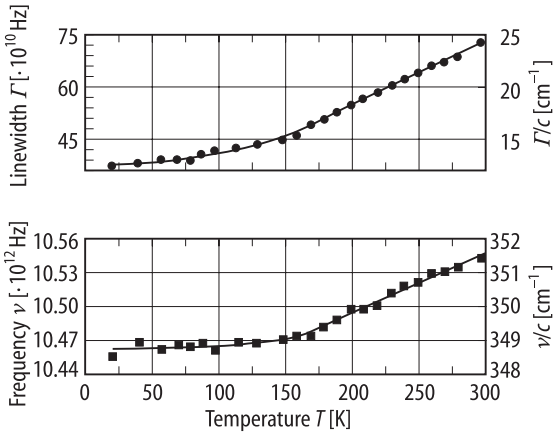

Fig. 33B-5-051. $Rb_{1-x}(ND_4)_xD_2PO_4$ (DRADP, x = 0.50). ν, Γ vs. T [95Yuz]. ν, Γ: Raman frequency and halfwidth of ν_2^P mode in $Y(ZZ)X$ geometry. See Table 33B-5-002.

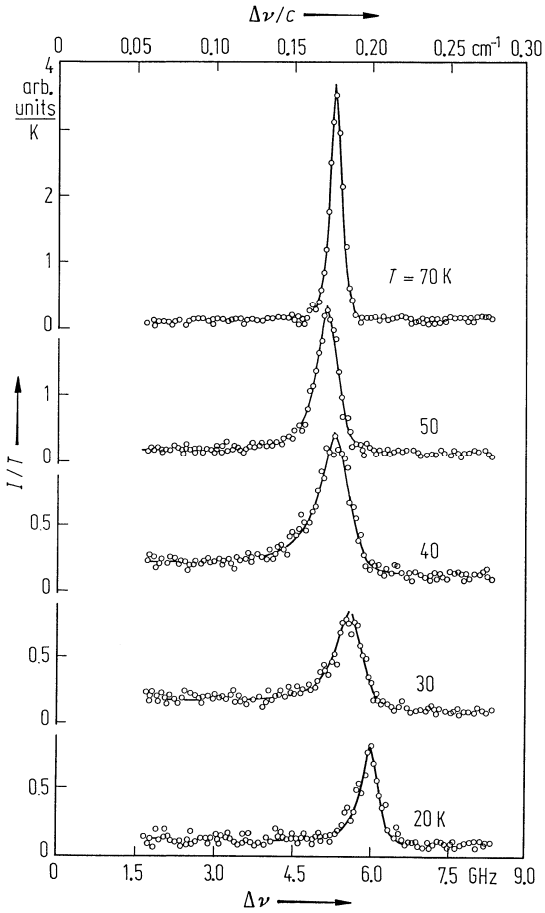

Fig. 33B-5-052. $Rb_{1-x}(NH_4)_xH_2PO_4$ (RADP, x = 0.35). I/T vs. $\Delta\nu$ [86Cou1]. Parameter: T. λ = 514.5 nm. I: Brillouin scattering intensity of the shear wave propagating along the a axis and polarized along the b axis. $\Delta\nu$: Brillouin frequency shift.

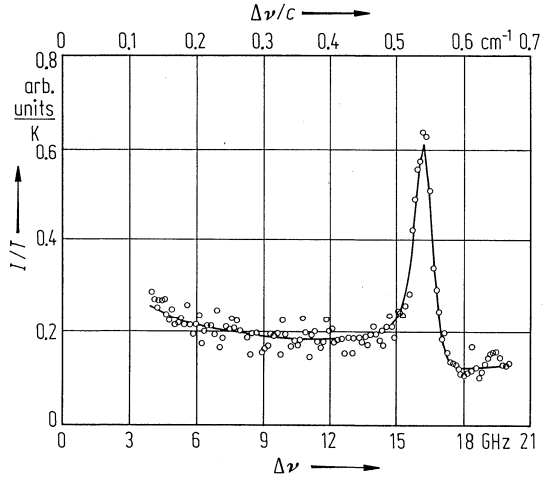

Fig. 33B-5-053. $Rb_{1-x}(NH_4)_xH_2PO_4$ (RADP, x = 0.35). I/T vs. $\Delta\nu$ [86Cou1]. λ = 514.5 nm. I: Brillouin scattering intensity of the longitudinal wave propagating along [110] at 38 K. $\Delta\nu$: Brillouin frequency shift.

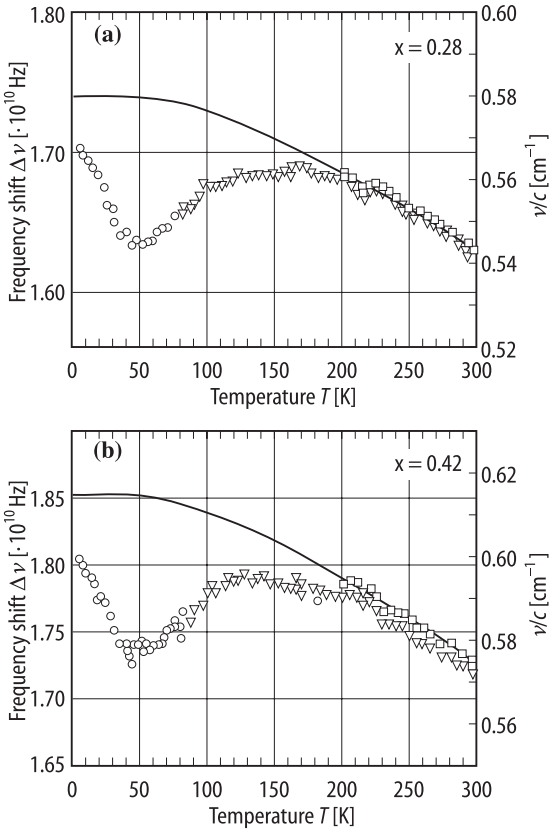

Fig. 33B-5-054. $Rb_{1-x}(NH_4)_xH_2PO_4$ (RADP, x = 0.28, 0.42). $\Delta\nu$ vs. T [91Bou]. $\Delta\nu$: Brillouin frequency shift of LA [110] phonon. Open circle: data taken with liquid He; open triangle: data taken with liquid N_2; open square: calculated bare phonon frequency. Full line: theoretical Debye curve. (**a**) x = 0.28, (**b**) x = 0.42.

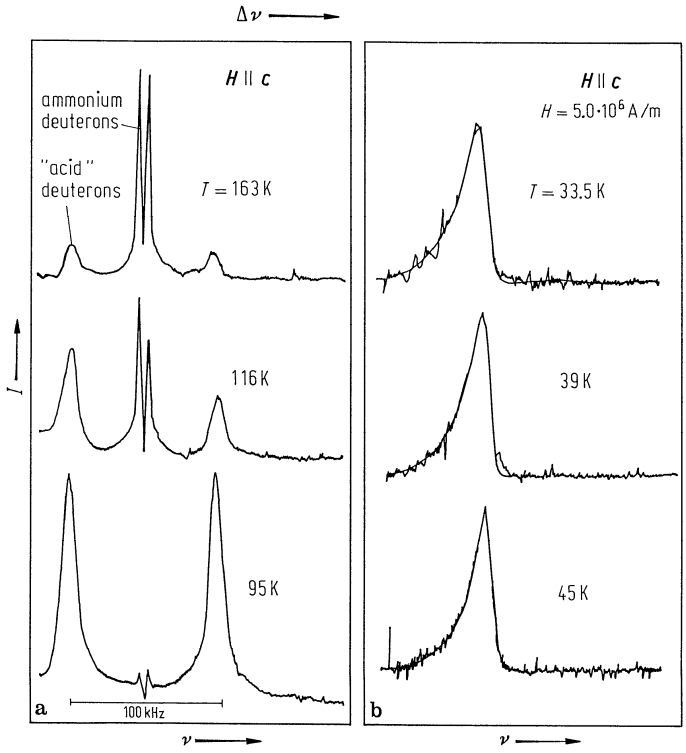

Fig. 33B-5-055. $Rb_{1-x}(ND_4)_xD_2PO_4$ (DRADP, x = 0.55). (**a**) Deuteron and (**b**) ^{87}Rb NMR spectra [86Bli]. Parameter: *T*.

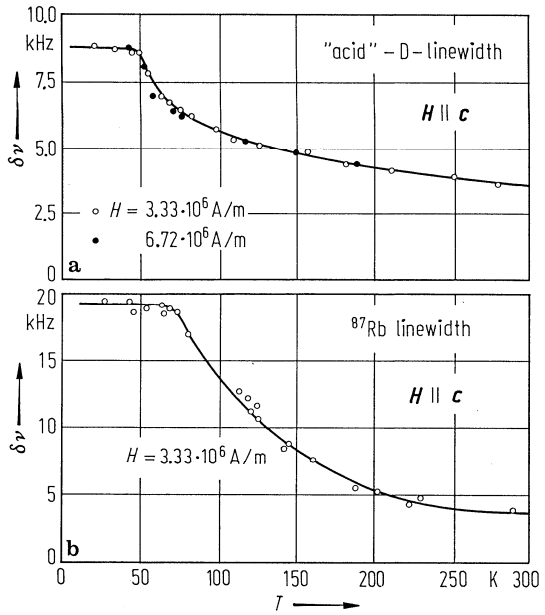

Fig. 33B-5-056. $Rb_{1-x}(ND_4)_xD_2PO_4$ (DRADP, x = 0.55). $\delta\nu$ vs. *T* [86Bli]. $\delta\nu$: linewidth of the (**a**) O–D...O deuteron and (**b**) ^{87}Rb 1/2 ↔ –1/2 NMR line. Deuteration rate: 70 %.

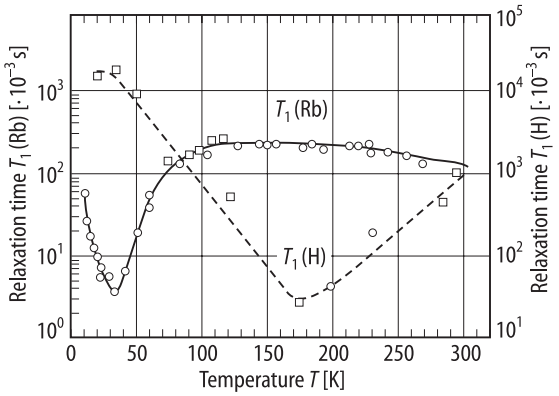

Fig. 33B-5-057. $Rb_{1-x}(NH_4)_xH_2PO_4$ (RADP, x = 0.35). T_1 vs. T [84Sla]. T_1: spin-lattice relaxation time of ^{87}Rb and ^1H. ν_L = 30.78 MHz. $\boldsymbol{c} \parallel \boldsymbol{H_0}$.

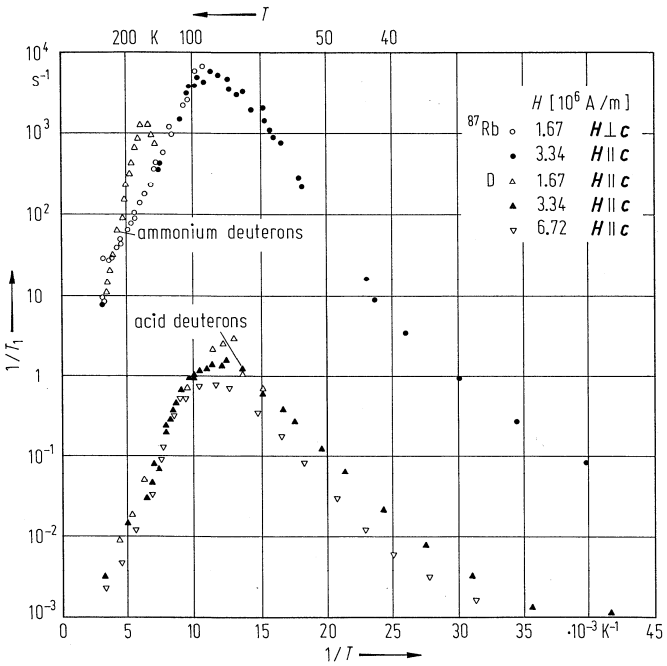

Fig. 33B-5-058. $Rb_{1-x}(ND_4)_xD_2PO_4$ (DRADP, x = 0.55). T_1^{-1} vs. T^{-1} [86Bli]. T_1: deuteron and ^{87}Rb 1/2 ↔ –1/2 spin-lattice relaxation time. Deuteration rate: 70%.

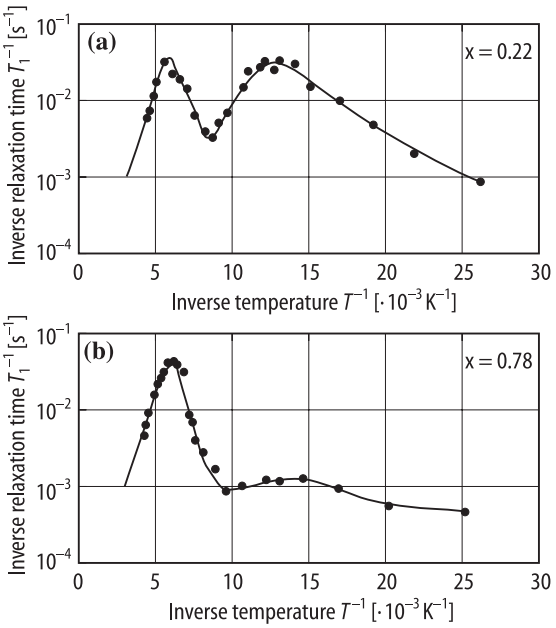

Fig. 33B-5-059. $Rb_{1-x}(ND_4)_xD_2PO_4$ (DRADP, x = 0.22, 0.78). T_1^{-1} vs. T^{-1} [93Che]. T_1: ^{31}P spin-lattice relaxation time. ν_L = 32.5 MHz. (**a**) x = 0.22, (**b**) x = 0.78.

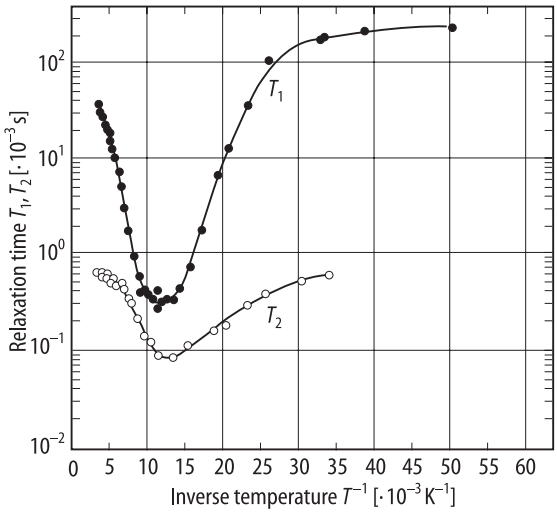

Fig. 33B-5-060. $Rb_{1-x}(ND_4)_xD_2PO_4$ (DRADP, x = 0.44). T_1, T_2 vs. T^{-1} [91Dol]. T_1: spin-lattice relaxation time of ^{87}Rb. T_2: spin-spin relaxation time of ^{87}Rb. ν_L = 88.34 MHz. $\boldsymbol{c} \parallel \boldsymbol{H}$.

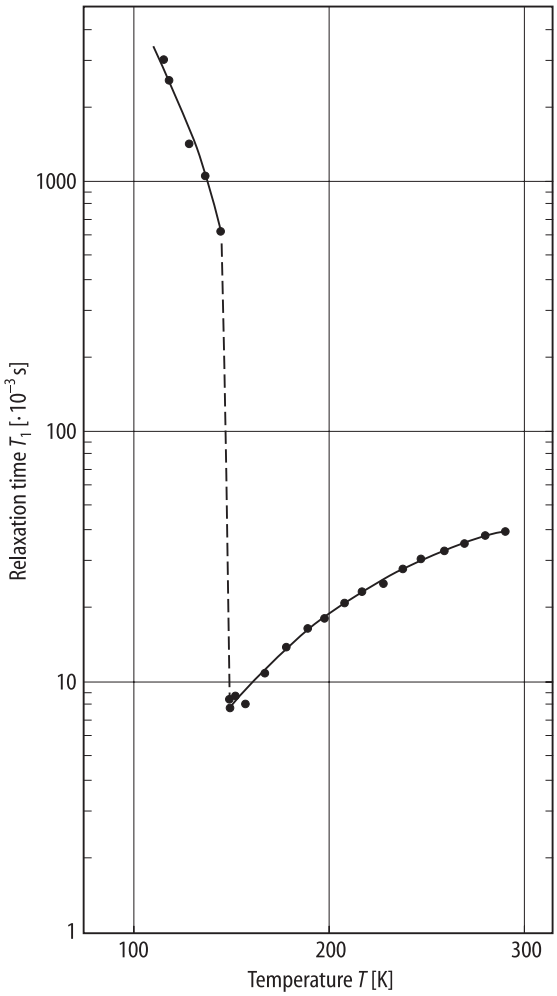

Fig. 33B-5-061. $Rb_{1-x}(ND_4)_xD_2PO_4$ (DRADP, x = 0.78). T_1 vs. T [87Kin]. T_1: ^{87}Rb spin-lattice relaxation time. ν_L = 88.346 MHz. $\boldsymbol{c} \parallel \boldsymbol{H}$.

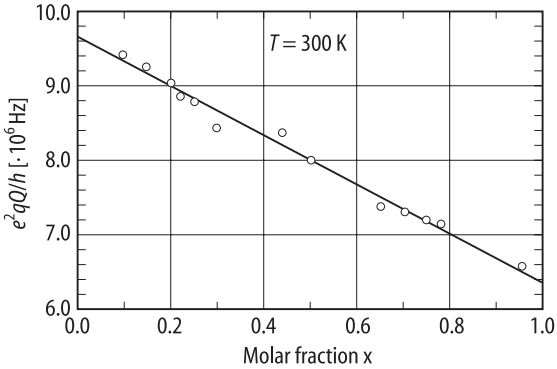

Fig. 33B-5-062. $Rb_{1-x}(ND_4)_xD_2PO_4$ (DRADP). e^2qQ/h vs. x [94Kor]. T = 300 K. e^2qQ/h: nuclear quadrupole coupling constant of ^{87}Rb.

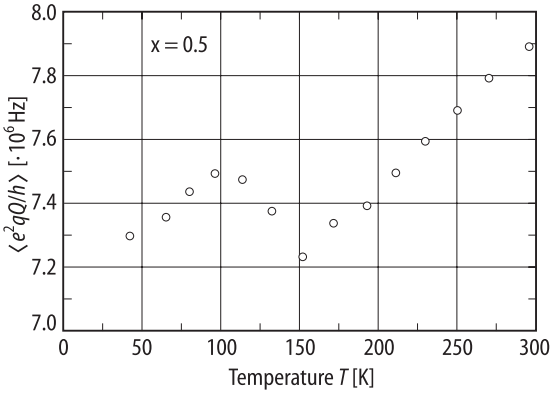

Fig. 33B-5-063. $Rb_{1-x}(ND_4)_xD_2PO_4$ (DRADP, x = 0.5). $\langle e^2qQ/h\rangle$ vs. T [94Kor]. $\langle e^2qQ/h\rangle$: mean nuclear quadrupole coupling constant for ^{87}Rb.

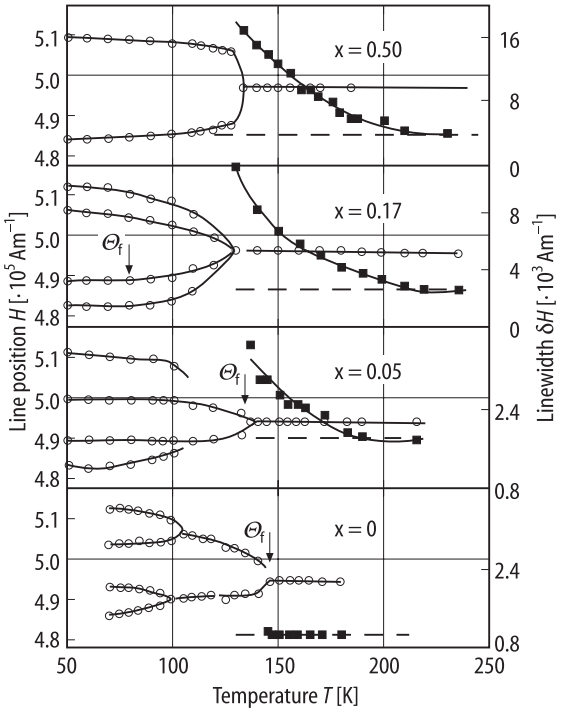

Fig. 33B-5-064. $Rb_{1-x}(NH_4)_xH_2PO_4$:Tl. H, δH vs. T [93Gri]. Parameter: x. H: magnetic field of Tl^{2+} ESR line. δH: linewidth of Tl^{2+} ESR line. Open circle: position of the resonance line; full square: line width. $\boldsymbol{H} \parallel \boldsymbol{a} + 45°$ for x = 0.50. $\boldsymbol{H} \parallel (\boldsymbol{a} + 45°) + 20°$ to $\boldsymbol{c}$ for x = 0, 0.05, 0.17.

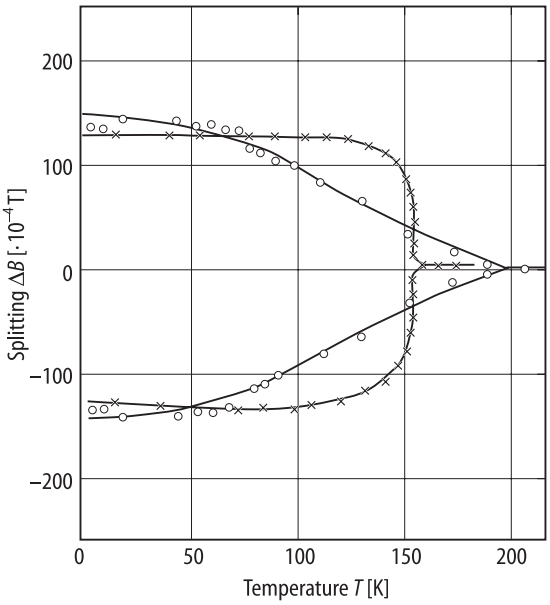

Fig. 33B-5-065. $Rb_{1-x}(NH_4)_xH_2PO_4$:Tl (x = 0.48). ΔB vs. T [89Cev]. ΔB: splitting of Tl^{2+} ESR low field line. $\boldsymbol{B_0} \perp \boldsymbol{c}$, $\boldsymbol{B_0} \parallel \boldsymbol{a}$. The results for RbH_2PO_4:Tl are shown for comparison. Open circle: RADP, cross: RDP.

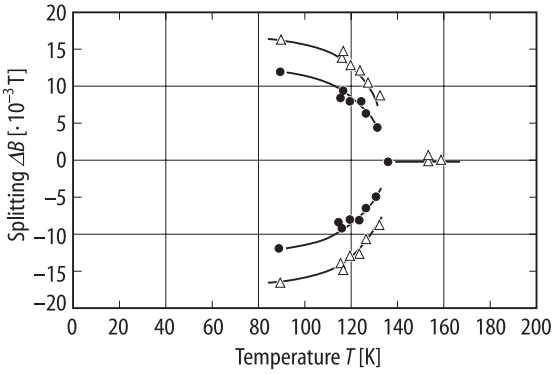

Fig. 33B-5-066. $Rb_{1-x}(NH_4)_xH_2PO_4$:Tl (x = 0.43). ΔB vs. T [91Kin]. ΔB: splitting of Tl^{2+} ESR line. $\boldsymbol{B_0} \parallel \boldsymbol{a} + 45°$. Full circle: low field line, open triangle: high field line.

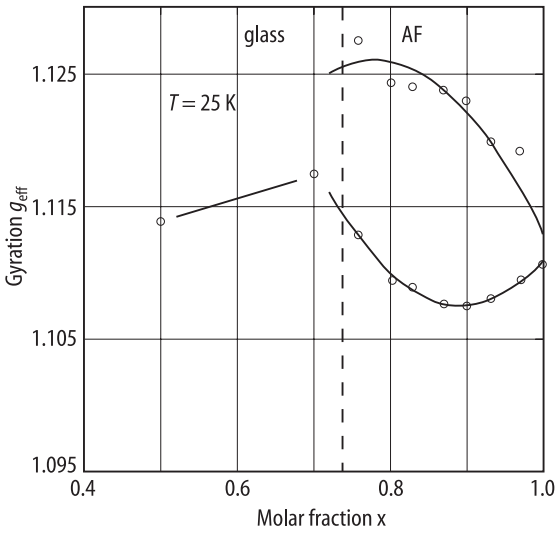

Fig. 33B-5-067. $Rb_{1-x}(NH_4)_xH_2PO_4$:Tl. g_{eff} vs. x [93Gri]. T = 25 K. g_{eff}: effective g-factor for Tl^{2+} center.

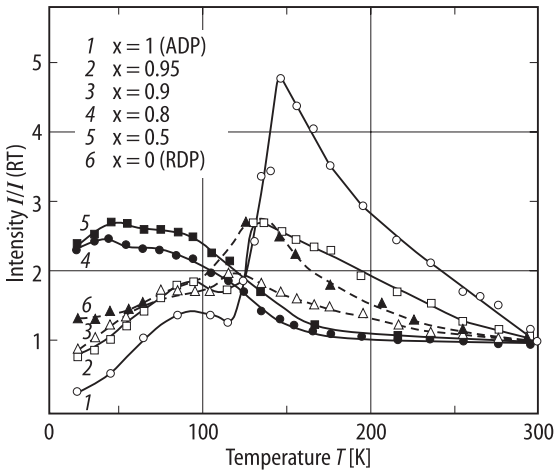

Fig. 33B-5-068. $Rb_{1-x}(NH_4)_xH_2PO_4$:AsO_4 (γ-irradiated). I/I(RT) vs. T [92Bab]. Parameter: x. I: intensity of ESR spectra of AsO_4^{4-}. I(RT): I at T = RT.

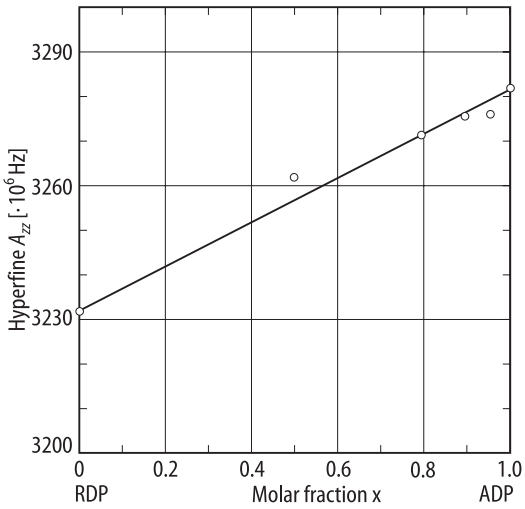

Fig. 33B-5-069. $Rb_{1-x}(NH_4)_xH_2PO_4$:AsO_4 (γ-irradiated). A_{zz} vs. x [92Bab]. A_{zz}: z-component of hyperfine coupling constant of ^{75}As due to AsO_4^{4-} radical.

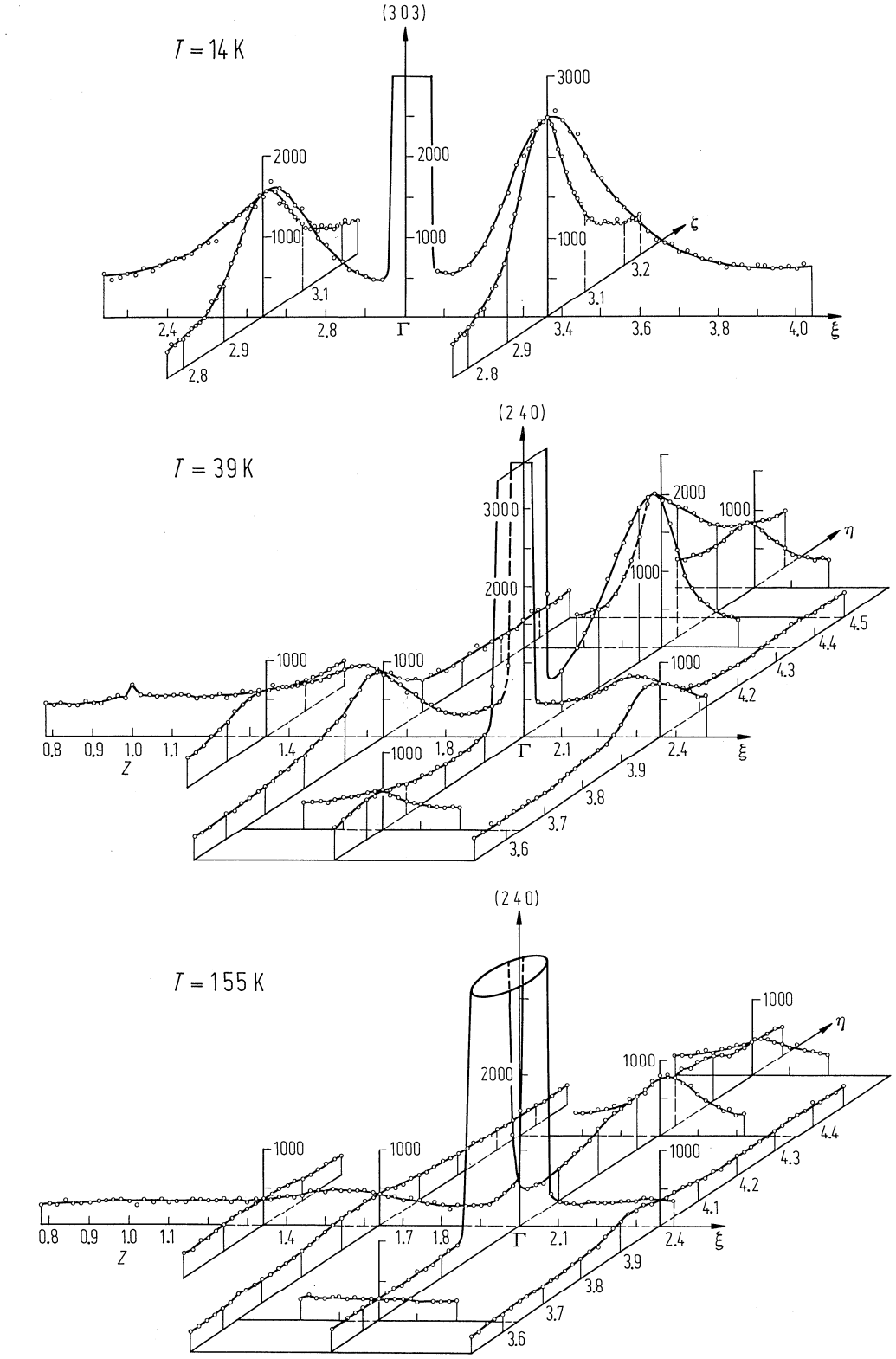

Fig. 33B-5-070. $Rb_{1-x}(ND_4)_xD_2PO_4$ (DRADP, x = 0.62). Intensity of diffuse scattering close to (303) and (240) [86Gri2].

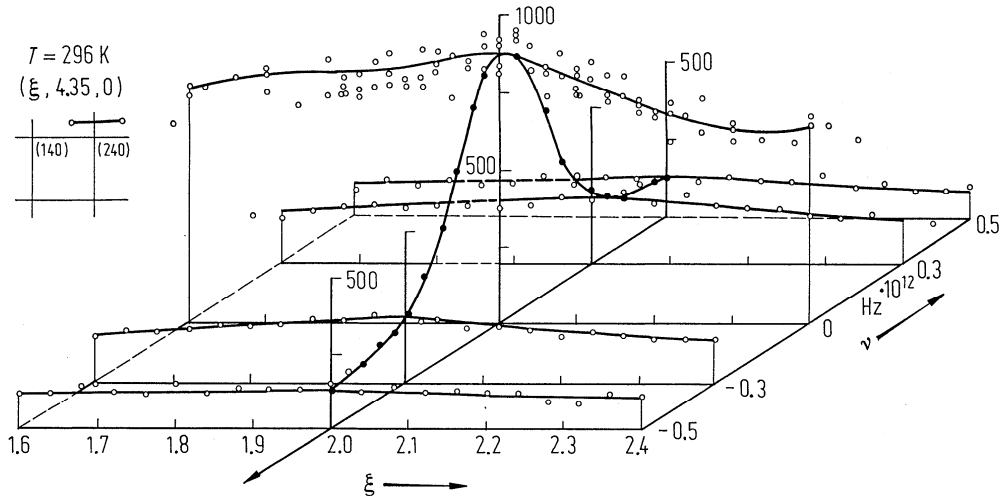

Fig. 33B-5-071. $Rb_{1-x}(ND_4)_xD_2PO_4$ (DRADP, x = 0.62). Diffuse scattering near (2, 4.35, 0) at T = 296 K together with its energy variation [86Gri2]. Insert indicates the scan path in reciprocal space.

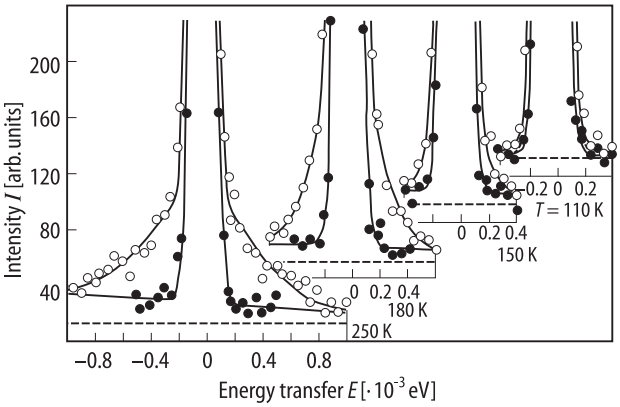

Fig. 33B-5-072. $Rb_{1-x}(ND_4)_xD_2PO_4$ (DRADP, x = 0.62). I vs. E [86Gri1]. Parameter: T. I: intensity of neutron scattering at the peak position (2, 1.65, 0) (open circle), and the reference position (2.52, 0.6, 0) (full circle). E: energy transfer. Dashed line: detector background.

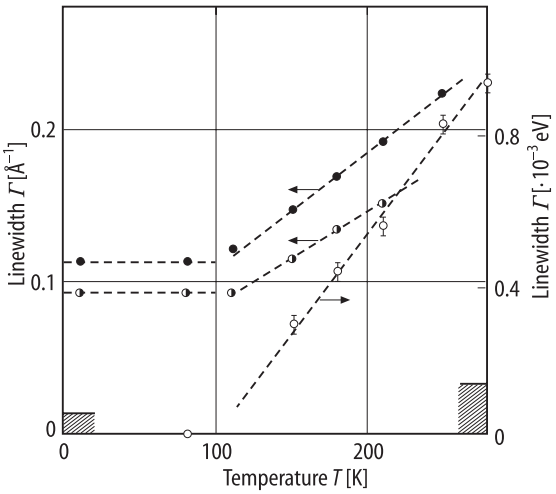

Fig. 33B-5-073. $Rb_{1-x}(ND_4)_xD_2PO_4$ (DRADP, x = 0.62). Γ vs. T [86Gri1]. Γ: full-width-half-maxima of the peak of neutron diffuse scattering through the position (2, 1.65, 0). Scan directions are ⟨001⟩ (full circles), ⟨100⟩ (half filled circles) and energy (open circles). The shaded levels indicate the relevant FWHM of resolution in momentum- (left) and energy-directions (right).

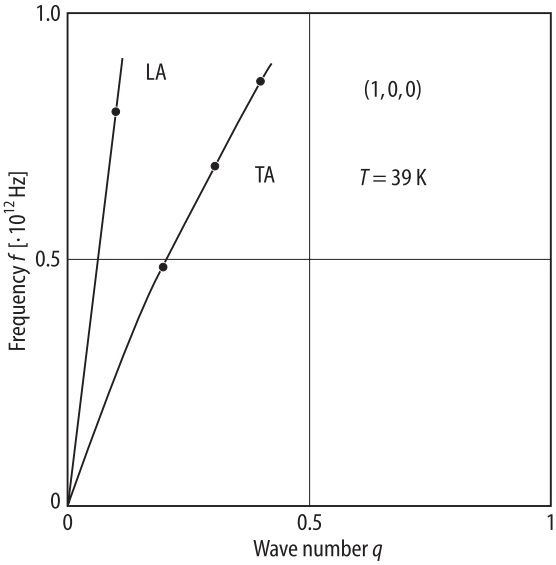

Fig. 33B-5-074. $Rb_{1-x}(ND_4)_xD_2PO_4$ (DRADP, x = 0.62). f vs. q [86Gri2]. f: frequencies of acoustic phonon with polarization vectors within the (h, k, 0) plane. q: wave number in the unit of $2\pi/a$. T = 39 K.

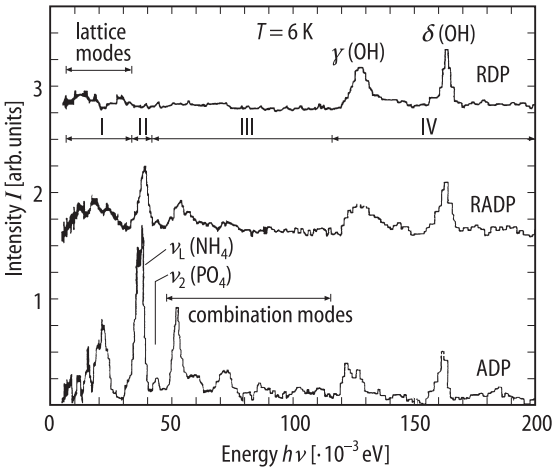

Fig. 33B-5-075. $Rb_{1-x}(NH_4)_xH_2PO_4$ (RADP, x = 0.35), RbH_2PO_4 (RDP), $NH_4H_2PO_4$ (ADP). I vs. $h\nu$ [90Goy]. I: intensity of neutron incoherent inelastic scattering.